1975

Bed and contact resistances in an electrically conducting fluidized bed

Tan-Ping Chen
Iowa State University

INFORMATION TO USERS

This material was produced from a microfilm copy of the original document. While the most advanced technological means to photograph and reproduce this document have been used, the quality is heavily dependent upon the quality of the original submitted.

The following explanation of techniques is provided to help you understand markings or patterns which may appear on this reproduction.

1. The sign or "target" for pages apparently lacking from the document photographed is "Missing Page(s)". If it was possible to obtain the missing page(s) or section, they are spliced into the film along with adjacent pages. This may have necessitated cutting thru an image and duplicating adjacent pages to insure you complete continuity.

2. When an image on the film is obliterated with a large round black mark, it is an indication that the photographer suspected that the copy may have moved during exposure and thus cause a blurred image. You will find a good image of the page in the adjacent frame.

3. When a map, drawing or chart, etc., was part of the material being photographed the photographer followed a definite method in "sectioning" the material. It is customary to begin photoing at the upper left hand corner of a large sheet and to continue photoing from left to right in equal sections with a small overlap. If necessary, sectioning is continued again — beginning below the first row and continuing on until complete.

4. The majority of users indicate that the textual content is of greatest value, however, a somewhat higher quality reproduction could be made from "photographs" if essential to the understanding of the dissertation. Silver prints of "photographs" may be ordered at additional charge by writing the Order Department, giving the catalog number, title, author and specific pages you wish reproduced.

5. PLEASE NOTE: Some pages may have indistinct print. Filmed as received.

Xerox University Microfilms
300 North Zeeb Road
Ann Arbor, Michigan 48106

Bed and contact resistances in an electrically conducting fluidized bed

by

Tan-Ping Chen

A Dissertation Submitted to the

Graduate Faculty in Partial Fulfillment of

The Requirements for the Degree of

DOCTOR OF PHILOSOPHY

Department: Chemical Engineering and Nuclear Engineering
Major: Chemical Engineering

Approved:

Signature was redacted for privacy.

In Charge of Major Work

Signature was redacted for privacy.

For the Major Department

Signature was redacted for privacy.

For the Graduate College

Iowa State University
Ames, Iowa

1975

TABLE OF CONTENTS

INTRODUCTION

Fluidized beds are well known as reactors for solid-gas reactions. Due to the mixing caused by fluidization, an intimate contact between gas and solid particles can be achieved as well as a fairly uniform temperature distribution over the entire bed. If the solid phase is composed of electrically conducting particles, passage of current through it will make the whole bed act as a resistance heater. This is one way to provide internally the process heat required for the chemical reactions and this type of reactor is called the electrofluid bed.

The current shortage of natural gas has stimulated active research aimed at obtaining substitutes for natural gas by various coal gasification processes. One major reaction involved in these processes is the carbon-steam reaction. It is highly endothermic and is usually carried out in a fluidized bed. Conventionally, the large amount of heat required for this reaction is provided either by transferring heat through the wall of the fluidized bed or by burning some of the coal being processed. The first method turns out to be inefficient when the quantity of heat being dealt with is large, while the second method causes the problem of contamination from flue gases generated in the partial combustion step. Use of an electrofluid bed which gives direct heating in the reaction zone tends to eliminate these two problems.

Proper design of an electrofluid bed depends on understanding its electrical characteristics. Work in this area has been carried out for several years at Iowa State University. In the study reported

here, calcined coke and graphite of different particle sizes were fluidized at room temperature with nitrogen with which no chemical reaction is anticipated. Therefore, the dependence of the electrical properties on the physical features of the fluidized bed could be singled out.

As indicated from experimental observations, the electrical resistance between a pair of electrodes in a fluidized bed has three components in series; contact resistances at the surface of each electrode and the bed resistance. Contact resistance is similar to the film resistance arising in problems of interphase heat or mass transfer. A large contact resistance usually will cause localized heating in the vicinity of the electrode while the rest of the bed stays rather cool. In the case of coal gasification, the electrodes even can soften and combine with the ash left by the reaction of the coal to form a nonconducting layer over the electrode surface. Both situations give very poor performance of the electrofluid bed. Part of the experimental work in this study was designed to explore the causes of contact resistance. Five factors which might affect the contact resistance were investigated. They were current density, fluidization velocity, type of bed material, electrode size (diameter) and the type of material used for the electrodes; stainless steel, silicon carbide, brass and graphite electrodes were tried.

Another major purpose of the study was to find a correlation for the bed resistivity. It was started out by visualizing the electrofluid bed as a composite material having solid, conducting particles contained in a nonconducting fluidizing gas and trying to apply Bruggeman's theory

of composite material to this model. However, since Bruggeman's theory is valid only when the continuous medium part of the composite material is rather electrically conducting, it was necessary to improve our model further. The static bed was then chosen as a fictitious continuous medium. As gas starts to flow, some bed particles lose contact with their neighbors and the conducting chains which account for the current flow are interrupted. Now regions occupied by these particles can no longer play a role in current flow. It followed that the whole bed can now be simulated by the introduction of nonconducting particles in a fairly conducting continuous medium and this model would then meet the requirements for applying Bruggeman's theory. The volume fraction of these fictitious nonconducting particles was believed to be a function of the relative fluidization velocity only. Experimental data were collected in order to justify this proposed model. As the basic structure of the static bed is totally destroyed when gas bubbles start to rise, the model just mentioned cannot be extended beyond that stage.

Experiments were also designed in this study to understand the effects of various factors on bed resistivity through the whole fluidization range. Those factors were bed material, bed particle size distribution and current density.

A method for predicting the potential and current fields in electrofluid beds was developed by Knowlton (27). In this investigation the same technique was extended to the beds possessing the contact resistances. Results from such analysis would then give an idea how the contact resistances affect the fields and the distribution of heat dissipation in electrofluid beds.

LITERATURE REVIEW

Over a thousand papers concerned with fluidization have been published. Several books (5, 29, 32, 52) can provide an excellent view on this subject. Only the investigations related to the electrofluid bed and the theory of composite materials will be reviewed here.

The Electrofluid Bed

The first use of an electrofluid bed was by Wickenden and Okell (48) in 1927 to produce decolorizing carbon; a bed of calcined vegetable carbon was fluidized by a combined stream of carbon dioxide and steam. A few years later a second application was suggested by Winkler (49) for the manufacture of water gas. Neither of these inventions were used in commercial production.

In the 1950's the electrofluid bed was developed into a practical tool by the Shawinigan Chemicals Division of Gulf Oil Canada Limited. A series of patents were issued for the adaptation of this special kind of reactor to the manufacture of hydrogen cyanide (20, 25, 26), carbon disulfide (18, 22), carbon monoxide (19), titanium tetrachloride (21) and olefine (28). More details about each process were released in several later articles (6, 10, 17, 38, 44). Two commercial plants were built for the production of hydrogen cyanide, one in Canada and the second in South Africa. They consisted basically of a bed of calcined petroleum coke fluidized by a gas mixture of ammonia and a hydrocarbon. (Usually it was propane, however, commercial natural gas could also be used.) The bed was heated to 1000-1500°C by the passage

of electric current between a pair of electrodes immersed in the bed. Due to the high temperature created inside the bed, ammonia reacted with the hydrocarbon directly without the introduction of expensive Plantium catalyst which was required in the conventional Andrussow process.

Many other applications of electrofluid beds have been suggested in recent years. Paquet and Foulkes (40) outlined the main features of their one-ton per hour pilot plant which was built to calcine petroleum coke. Goldberger, Hanway and Langston (10) reported that operation of their laboratory scale electrofluid bed at temperatures up to 8000°F was possible and enumerated its potential use in areas such as metallurgy and a variety of chemical processing. Miles and Stephens (36) patented a process for the preparation of phosphorus from shale. In this process, shale was crushed into finely divided powder and was then fluidized by a hydrocarbon gas. As the temperature was raised by current flow inside the bed, shale decomposed into calcium silicate gangue and elemental phosphorus. In developing a pilot plant for making substitute natural gas, the Institute of Gas Technology (30) utilized an electrofluid bed as an integral part of the process equipment to convert the residual coal char from the main gasifier into a hydrogen-rich gas by reaction with steam. Hydrogen thus produced was then used to raise the H/C ratio of the reactant gas in the subsequent methanation process. Their reactor was operated in the temperature range of 1500-1900°F and at a pressure up to 1000 psig. Similar studies have been carried out at Iowa State University (41), but the operation was at atmospheric pressure.

Electrical properties of electrofluid beds

The search for an understanding of the electrical characteristics of electrofluid beds is still in the pioneer stage. Numerous experiments have been conducted to determine the dependency of electrical properties on fluidization conditions and the modes of conducting electric power in the bed. So far no successful correlation has been developed, nevertheless some general conclusions can be drawn from information provided by these experiments.

In 1963 Goldschmidt and LeGoff (11) examined three possible mechanisms for current flow through the bed. They were:

1. current flow along continuous chains of particles,
2. diffusion type of current flow where electric charges are shared between colliding particles,
3. arcing in the gas phase between particles.

By analogy with the theory of heat transfer, electrical resistivity predicted by the second mechanism was shown to be several orders greater than the measured one. It is therefore generally accepted that a diffusion type of current flow is not possible. Graham and Harvey (13) observed that cyanogen was absent in the off-gas when their coke bed was fluidized by nitrogen with current of not more than 30 amperes. Therefore, they concluded that at low current densities arcing is not significant and current flow is primarily through conducting chains of solid particles. Further support of this conclusion was given by Reed and Goldberger (42) as they found that in the temperature range of 600 to 1000°C the type of fluidizing gas did not have a noticeable effect on the electrical resistivity. This would

not be true if arcing did occur. However, at higher current densities and temperatures, Johnson (17) noted the appearance of sparks as a result of arcing which together with conducting chains, was believed to account for the current flow under such conditions. Lee, et al. (31) reported that at a pressure of 1000 psi, their char bed was in a state of particulate fluidization and the main mechanism for current flow under such a condition was through arcing. Zheltov et al. (53) proposed that arcing between particles caused by photoionization could play a considerable role in the conduction of current through a bed at very high temperatures.

From a measurement of the potential profile inside an electrofluid bed, Reed and Goldberger (42) noticed there were voltage drops at the surfaces of the electrodes. This indicated that the interelectrode resistance was partially due to contact resistance at the electrodes. Since then several techniques have been devised to detect bed resistance and contact resistance separately such as the probe or screen method (42, 51), the four terminal method (9, 23, 24, 45) and the electrolyte cell method (14). Instead of reporting the contact and bed resistances individually, some research workers measured only the sum of these two resistances. Experimental conditions used by researchers who have dealt with the resistances of electrofluid beds are summarized in Table 1. These investigations have dealt with, at least qualitatively, the effects of the following factors:

1. fluidization velocity
2. type of fluidizing gas
3. operating temperature

Table 1. Summary of experimental work concerning electrofluid beds

Author	Ballain and Pulsifer (1)	Glidden and Pulsifer (9)
Temperature	1200°F	Room temperature
Pressure	Atmospheric pressure	Atmospheric pressure
Bed material	Coal char, d_p = 0.0087 and 0.0168 inches	Calcined coke; -48+65, -65+100, and -100+150 mesh
Reactor and electrodes	4 inch I.D. stainless steel tube; reactor wall as one electrode, 0.5 inch diameter stainless steel rod as the center electrode.	6 inch I.D. Plexiglass tube; two pieces of copper band as wall electrode, graphite rods, 0.5, 1, 1.5 inches in diameter, as center electrode.
Fluidizing gas	Nitrogen	Nitrogen
Factors investigated	Temperature difference between bed and center electrode, voltage gradient, flowrate, electrode immersion; electrical property measured was inter-electrode resistance.	Flowrate, center electrode diameter, current density, particle size; electrical property measured was contact resistance.

Table 1. Continued

Goldschmidt and LeGoff (11)	Graham and Harvey (13)	Graham and Harvey (14)
Room temperature	Room temperature	Room temperature to 1200°C
Atmospheric pressure	Atmospheric pressure	Atmospheric pressure
Sulfonated polystyrene spheres; d_p = 73 μ Nickel spheres; d_p = 80-160 μ Carbon spheres; d_p = 600-800 μ	Coke; -48+65, -65+100, -100+150, and -150+200 mesh Graphite; -48 + 65, -65+100, -100+150, and -150+200 mesh	Coke; -35+80 mesh Graphite; -35+80 mesh
Glass column, I.D. = 10 cm or 5 cm; two copper plates with a surface area of 14 cm^2 stuck to the inner wall surface as electrodes.	2 inch I.D. column, 1.5 X 3 inch column, 8 X 4 inch column; two graphite rods inserted as electrodes.	4 inch I.D. column; two graphite rods, 0.5 inches in diameter as electrodes.
Air	Air	Nitrogen
Flowrate, column diameter, particle size, bed material; electrical property measured was interelectrode resistance.	Flowrate, particle shape, position of electrodes from the distributor; electrical property measured was interelectrode resistance.	Flowrate, particle shape, temperature, bed material, electrical property measured was bed resistivity.

Table 1. (Continued)

Jones and Wheelock (23)	Lee et al. (31)	Reed and Goldberger (42)
Room temperature	1350-1900°F	25°C, 600°C, 1000°C
Atmospheric pressure	1 atm to 1000 psi	Atmospheric pressure
Calcined coke; -65+250 mesh Graphite; -65+250 mesh	Coal char; d_p = 0.0095 inches	Graphite; -35+150 mesh
2 or 4 inch I.D. column; two copper foils located at bottom and upper section of the bed as the electrodes.	4 inch I.D. column; 0.5 inch diameter stainless steel rod as center electrode, wall of column as another electrode.	2 X 4 inch rectangular column, 2 inch I.D. column; in the first reactor, two copper plates placed at opposite walls as electrodes, in the second column, 0.25 inch diameter graphite rod as center electrode and a nichrom screen at the wall as another electrode.
Nitrogen	Nitrogen mixed with steam	Nitrogen, argon, carbon monoxide
Flowrate, particle size distribution, bed material, particle size; electrical property measured was bed resistivity.	Pressure, current density; electrical property measured was bed resistivity[a].	Flowrate, temperature, current density, type of gas, vibration effect. Both bed resistivity and contact resistance were measured.

[a]Without the consideration of the possible existence of contact resistances.

Table 1. (Continued)

Sevryukov and Martyushin (43)	Smith (45)	Zheltov et al. (53)
Room temperature to 160°C	70-1500°F	25-2500°C
Activated carbon; 0.25-0.45 mm	Coal char; -48+65 mesh Calcined coke; -48+65 mesh	Graphite; -630+400, -355+315, -315+250, -200+160, -160+100, and -100+63 μ
4 inch I.D. column; stainless steel screen as wall electrode, stainless steel rod of 0.5 inch diameter as center electrode.	5.5 inch I.D. tube; stainless steel gas distributor as bottom electrode, stainless steel band stuck to wall surface as upper electrode.	10 inch I.D. column or 5 X 11 cm column; in the first reactor, graphite rod of 3 cm diameter as center electrode, in the second reactor, two graphite plates (5 X 12 cm) as electrodes.
Nitrogen	Nitrogen	Dry air, nitrogen, argon, helium
Electrode immersion, voltage gradient; electrical property measured was interelectrode resistance.	Temperature, flowrate, current density; electrical property measured was bed resistivity.	Flowrate, current density, temperature, amount of nonconducting material added, particle size, bed height, type of gas; electrical property measured was bed resistivity[a] and its amplitude and frequency of oscillation.

4. operating pressure
5. current density or voltage applied
6. type of bed material
7. average particle size
8. particle size distribution
9. bed height
10. bed diameter
11. type of electrode material
12. geometric arrangement of electrodes inside the bed
13. electrode size and shape

Experimental findings showed two patterns of the effect of fluidization velocity on the interelectrode or bed resistances. In the first pattern (1, 13, 14, 23), resistance increased from a minimum corresponding to the settled bed to a maximum value at a flowrate slightly over the minimum fluidization velocity, followed by a sharp decrease and finally a leveling off at higher gas velocities. Graham and Harvey (13) explained the drop-off after the peak by the decrease of voidage in the emulsion phase as bubbles started to form. In the second case, Graham and Harvey (14) noted that the resistance in a high temperature coke bed followed approximately the first pattern, but instead of leveling off at the higher gas velocity the resistance increased again. This was shown to be the result of the occurrence of significant arcing at the high temperature operating condition. However, the same deviation was not observed by these authors for the graphite bed because it had less tendency to arc at high temperature. In the second pattern (11, 12, 15, 42, 53), the resistance did not show any peak at all but

increased all the way from the settled to the completely fluidized bed with the largest rate of increase at the minimum fluidization velocity. The reasons for these two rather distinct patterns are not known.

In the discussion of any current density effect, the operating pressure and temperature under which the effects were investigated must be specified. As indicated by Lee et al. (31), the bed resistivity decreased as current density increased at high temperature and pressure. The same trend was observed at room temperature and atmospheric pressure by a number of research workers (9, 12, 42, 45, 53), but the dependency of resistance on current gradually diminished as the temperature increased.

Reed and Goldberger (42), Smith (45) and Zheltov et al. (53) all reported from their experimental results that the bed resistivity became smaller as temperature increased for both fixed and fluidized beds.

In contrast to this the effect of pressure was discussed only by Lee et al. (31). Their data showed a linear relationship between bed resistivity and pressure when both were plotted on a logarithm scale. However, the slope of the line was close to one when the measurements were carried out at a small, fixed current density and approached zero at large current densities. They attributed this to a change in the mechanism of current flow from a general type of arcing (Paschen's law) to field emission when the current density was increased.

Although Reed and Goldberger (42) claimed that the type of fluidizing gas had no effect on the bed resistivity at small current

density, Zheltov et al. (53) did find some difference between helium and argon. The bed resistivity obtained with helium as the fluidizing gas was higher than that with argon. This experimental observation, together with the fact that helium has a higher ionization potential (24.58 volts) than argon (15.755 volts), led them to consider photo-ionization as a possible mechanism for current flow.

Jones and Wheelock (24) and Zheltov, et al. (53) measured the bed resistivity at different bed heights. They found it decreased with larger bed heights, but this change was significant only for settled beds. Jones and Wheelock (24) also indicated that the bed resistivity increased as bed diameter decreased.

A common conclusion has been reached by various investigators of particle size effects. They (13, 23, 24, 53) stated that the bed resistivity decreased as the particle size increased. Further investigation of the effect of particle size distribution was reported by Jones and Wheelock (23). In their experiments, bed resistivity was measured for both a graphite bed and a calcined coke bed with different particle size distributions. It was found that the peak in the bed resistivity-flowrate data mentioned in the preceeding discussion of flowrate effects tended to be higher with a wider particle size distribution. When a comparison of the peak heights was made between the graphite bed and calcined coke bed with the same particle size distribution, the latter was higher which was probably due to the larger angle of repose of the coke particles. It is worthwhile here to point out a correlation proposed by Goldschmidt and LeGoff (11) as well as by Reed and Goldberger (42). They showed that a unique relationship

existed between the relative bed resistivity and the relative fluidization velocity (both were relative to the quantity measured at fluidization) for a given bed material no matter what the particle sizes were. This rather striking fact has not been explained based on any theoretical reasoning.

Very little study of the contact resistances has been reported in the literature. Reed and Goldberger (42) only mentioned that contact resistance had a tendency to decrease at higher current density. Glidden and Pulsifer (9) reported that no more than 2% of the interelectrode resistance of their system was contributed by contact resistance; their measurements were made in a calcined coke bed with a graphite rod as the center electrode.

Theory of Composite Materials

A heterogeneous system of particles dispersed in a continuous medium, such as slurries, foams and various porous beds, occurs frequently in chemical engineering problems. The physico-chemical properties of these mixtures are of interest to many research workers. Among these properties are the effective thermal and electrical conductivities which cannot be obtained by just averaging the corresponding properties of the pure phases (39). A large number of experimental measurements is presently available, but theoretical work in this field is surprisingly scarce. (For a review of the work done before 1962, see Meredith and Tobias (35).) This is due to the considerable mathematical difficulties encountered when attempting to solve the conduction

equations for this complex, many-bodied problem both within the continuous medium and inside the dispersed particles with proper boundary conditions at the interface.

The simplest kind of composite material consists of a dilute dispersion of spherical particles of conductivity K_d in a continuous medium of conductivity K_c. Because of the low concentration of the dispersed phase, interactions of the potential field between particles can be neglected. This simplicity enabled Maxwell (34) to derive an expression for the effective conductivity of the mixture, K_m, as:

$$K_m = K_c \frac{K_d + 2K_c - 2f(K_c - K_d)}{K_d + 2K_c + f(K_c - K_d)}, \qquad f < 0.1 \qquad (1)$$

where f is the volume fraction of the dispersed phase. In practice, it has been found that conductivity data may be accurately represented by the above equation both for random and ordered dispersions of spheres. However, for particle shapes other than spherical, this is not true. Fricke (8) has considered the case of randomly dispersed ellipsoidal particles; the expression derived for K_m reduces to equation (1) when all three principal axes of the ellipsoidal particles are equal.

Although one is not able to tell the difference between the effective conductivity of random and ordered arrangements of particles for highly dilute dispersions, these factors do require some consideration when the concentration of the dispersed phase is increased. Lord Rayleigh (33) treated the case of uniformly sized spheres in cubic lattice positions. Using the principle of superposition of potentials, he got:

$$\frac{K_m}{K_c} = 1 - \frac{3fK_c}{(2K_c + K_d)/(K_c - K_d) + fK_c - 0.525(K_c - K_d)f^{10/3}/(\frac{4}{3}K_c + K_d) + \ldots} \qquad (2)$$

For randomly dispersed particles at high concentration, Bruggeman (2) developed a technique called the "self-consistent scheme" to approach the problem. First, he imagined that a composite material was constructed by adding infinitesimal amounts of particles successively to the continuous medium until the desired concentration of the dispersed phase was reached. With each addition, the mixture made in the preceeding stage was considered as a fictitious continuous medium. Since the amount of particles added each time was so small, the resulting effective conductivity after the addition was given by equation (1) except K_c now represented the conductivity of the fictitious continuous medium. Summing up the effects of each infinitesimal addition by integration, the final value of K_m obtained was:

$$1 - f = \frac{K_m - K_d}{(\frac{K_m}{K_c})^{1/3}(K_c - K_m)} \qquad (3)$$

A limitation of Bruggeman's approximation arises because a fictitious continuous medium is assumed and this is true only if the successively added particles are much larger than the ones added previously. This implies that in order to use equation (3), one must have a random dispersion of particles with wide size distribution.

Buyevich (3) recently adopted an alternative approach to the same problem so that the limitation set by Bruggeman's approximation could be removed. First, he considered any particle in a composite material

to be surrounded by a fictitious continuous medium which actually was the mixture of the original continuous medium and the rest of the dispersed particles. The conductivity of the fictitious medium was assumed to be a known value and this enabled him to calculate the change of conductivity due to the appearance of this particular particle. Since the dispersion of particles was completely random, it was possible to use a statistical treatment to superimpose the effect of all particles to find the conductivity of the fictitious medium. Equating this conductivity with the one formerly assumed, the effective conductivity was found to be:

$$\frac{K_m}{K_c} = h \frac{(7g + 17)h + 5g + 7}{(1 - f)[(7g + 17)h + 5g + 7] + 36fh} \qquad (4)$$

where $g = \frac{K_d}{K_c}$

and

$$h = \frac{(2+29f)g+10-17f+\{[(2+29f)g+10-17f]^2+4(1-f)(5g+7)(7g+17)\}^{1/2}}{2(7g+17)}$$

All the theories discussed so far are unsuitable for composite materials having a continuous medium of poor conductivity. This is because in their derivation the possibility of having conducting chains for current flow is ruled out. However, this is the main mechanism when the continuous phase is rather nonconductive. The conductance of packed spheres in vacuum (4, 50) is a problem in this category. Both Yovanovich (50) and Chan and Tien (4) obtained analytical expressions for the effective conductivity of orderly packed beds. As pointed out by Holm (16), current flow through contacts between particles

in a packed bed strongly depends on the load applied to the particles. The load can be from outside or just the weight of the bed itself.

The only application of composite material theory to fluidized beds was given by Turner (47). The bed consisted of a special kind of Na^+ ion-exchange resin bead fluidized particulately with sodium chloride solution. Data obtained agreed fairly well with Bruggeman's equation.

FIELD THEORY ANALYSIS OF FLUIDIZED BED RESISTANCE

A computer simulation of the potential field distribution inside the electrofluid bed will be presented in this section. Similar calculations have been done by Knowlton (27) except the existence of contact resistances will be considered here. Information available from such an analysis contributes to an understanding of the electrical field distortion due to the contact resistances as well as giving some information on where the heat is generated in the bed.

In order to apply field theory directly, it was necessary to assume that the bed resistivity was uniform over the entire electrofluid bed. In reality, an actual bubbling fluidized bed is not perfectly homogeneous nor is its resistivity invariant from moment to moment. However, over a long period of observation, the average properties of the bed should be nearly constant throughout the bed. The geometric configuration of the bed inside which the potential field was simulated is shown in Figure 1. In this system a conducting, cylindrical bed was in contact with a pair of concentric electrodes. The bed was 16 inches high and 6 inches in diameter. All of the 8-inch long center electrode was exposed to the bed. The potential field subject to this arrangement could be described by Laplace's equation:

$$\frac{\partial^2 \phi}{\partial r^2} + \frac{1}{r}\frac{\partial \phi}{\partial r} + \frac{\partial^2 \phi}{\partial z^2} = 0 \qquad (5)$$

with the following boundary conditions:

$$\frac{\partial \phi}{\partial r} + \frac{\rho_b}{\rho_{cw}}\phi = 0 \qquad \text{for } r = r_2 \text{ and } 0 \leq z \leq z_2$$

Figure 1. Cylindrical bed cross section

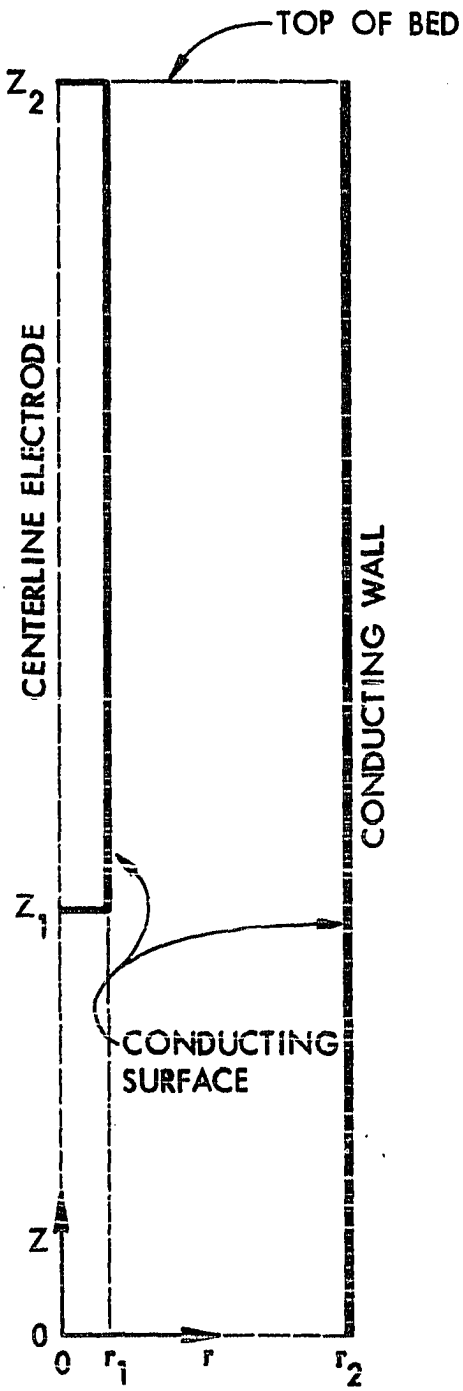
TOP OF BED
Z_2
CENTERLINE ELECTRODE
CONDUCTING WALL
Z_1
CONDUCTING SURFACE
Z
0
0
r_1
r
r_2

$$\frac{\partial \phi}{\partial r} - \frac{\rho_b}{\rho_{ce}} (\phi - 1) = 0 \qquad \text{for } r = r_1 \text{ and } z_1 \leq z \leq z_2$$

$$\frac{\partial \phi}{\partial z} + \frac{\rho_b}{\rho_{ce}} (\phi - 1) = 0 \qquad \text{for } z = z_1 \text{ and } 0 \leq r \leq r_1$$

$$\frac{\partial \phi}{\partial r} = 0 \qquad \text{for } r = 0 \text{ and } 0 \leq z \leq z_1$$

$$\frac{\partial \phi}{\partial z} = 0 \qquad \text{for } z = 0 \text{ and } 0 \leq r \leq r_2$$

$$\text{for } z = z_2 \text{ and } r_1 \leq r \leq r_2$$

where

ϕ = electrical potential, dimensionless

ρ_b = bed resistivity, ohm-inch

ρ_{cw} = contact resistivity at wall, ohm-inch^2

ρ_{ce} = contact resistivity at center electrode, ohm-inch^2

The first three boundary conditions were derived from a current balance across the electrode surface, while the last two are the standard condition for a nonconducting surface.

The current flow lines inside the bed were found by solving for the stream function from the following equation:

$$\frac{\partial^2 \psi}{\partial r^2} - \frac{1}{r} \frac{\partial \psi}{\partial r} + \frac{\partial^2 \psi}{\partial z^2} = 0 \qquad (6)$$

with boundary conditions:

$$\psi = 1 \qquad \text{for } z = z_2 \text{ and } r_1 \leq r \leq r_2$$

$$\psi = 0 \qquad \text{for } z = 0 \text{ and } 0 \leq r \leq r_2$$

$$\psi = \int_A \frac{1}{I\rho_b} \left(\frac{\partial \phi}{\partial n}\right) dA \qquad \text{at the surface of the electrodes}$$

where

$\frac{\partial \phi}{\partial n}$ = potential gradient normal to the surface

ψ = stream function

I = total current flow between electrodes

A = surface area of electrode

Two cases were considered with the sets of assumed resistivities shown in the first three lines of Table 2. Case I in the table is for a fairly high bed resistivity, 300 ohm-inches, while in Case II the bed resistivity is much lower, 30 ohm-inches. The contact resistivities are the same in both cases. Equations (5) and (6) were solved numerically by the Liebman four-point procedure in conjunction with an overrelaxation technique as described by Knowlton (27). This method provided values of the potential and stream functions at each point in a grid obtained by dividing the bed into 25 radial and 130 longitudinal increments. The equipotential lines and stream lines were then determined by linear interpolation. The calculated equipotential lines and stream lines for the right half of the bed are shown in Figure 2. These lines divide the bed region into increments such that 10% of the overall change across the bed in either the electrical potential or stream function occurs over each increment.

The equipotential lines are orthogonal to the stream lines in Figure 2 which is the expected result from field theory. Another feature shown in the same diagram is that the stream lines do not intersect the electrode surface at right angles because the electrode surfaces are no longer equipotential surfaces if contact resistance exists. In Case I where the majority of the interelectrode resistance is due

Table 2. Summary of the two cases considered for calculation of the electrical field with contact resistance

	Cases	
	I	II
Bed resistivity ρ_b, ohm-inch	300	30
Contact resistivity at center electrode ρ_{ce}, ohm-inch^2	20	20
Contact resistivity at wall electrode ρ_{cw}, ohm-inch^2	200	200
Total interelectrode resistance R_t, ohm	11.39	2.66
Contact resistance at center electrode R_{ce}, ohm	0.7	0.74
Contact resistance at wall electrode R_{cw}, ohm	1.02	0.86
Bed resistance R_b, ohm	9.67	1.06
Bed resistance with no contact resistance present, ohm	9.6	0.96

to the bed resistance, the equipotential lines and stream lines in the upper portion of the bed between the electrodes are fairly straight and parallel. However, in Case II these lines are curved even in this region of the bed.

Since the field is distorted due to the contact resistance, the overall contact resistance cannot be calculated by the following equation:

$$R_c = \frac{\rho_c}{A}$$

where

R_c = overall contact resistance

ρ_c = contact resistivity

A = electrode surface area

Figure 2. Electrical field for concentric bed with contact resistance

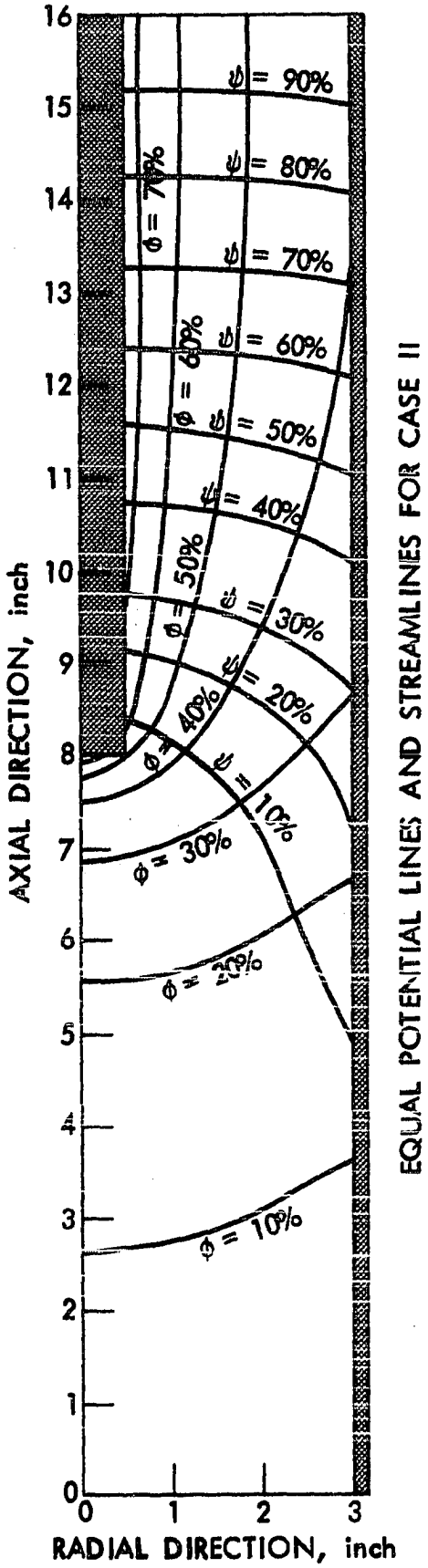
AXIAL DIRECTION, inch
RADIAL DIRECTION, inch
EQUAL POTENTIAL LINES AND STREAMLINES FOR CASE II
ψ = 90%
ψ = 80%
ψ = 70%
ψ = 60%
ψ = 50%
ψ = 40%
ψ = 30%
ψ = 20%
ψ = 10%
φ = 70%
φ = 60%
φ = 50%
φ = 40%
φ = 30%
φ = 20%
φ = 10%

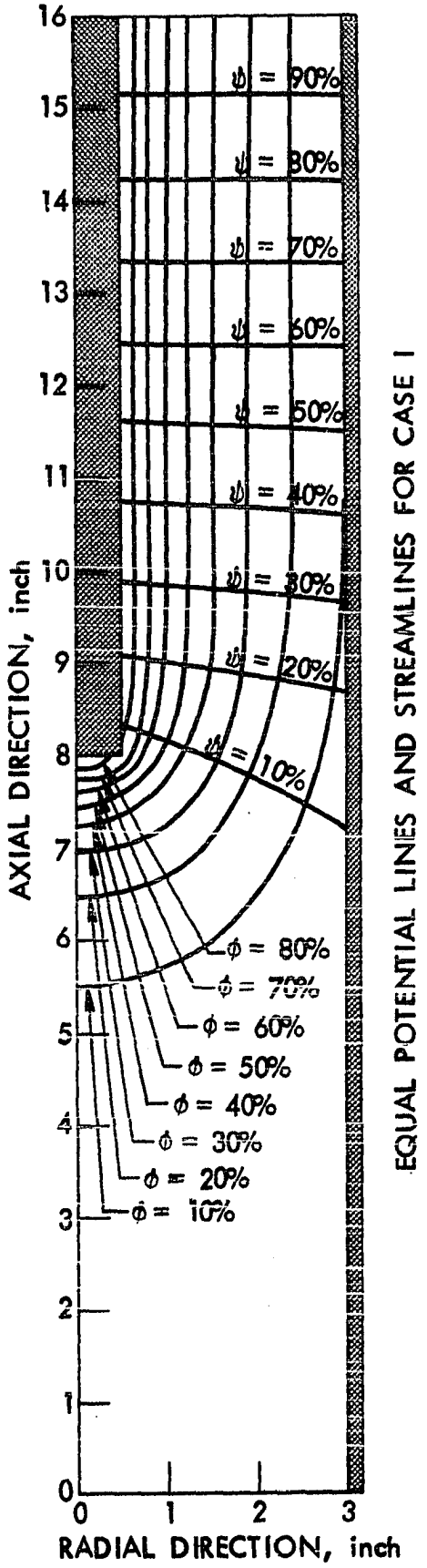
AXIAL DIRECTION, inch
RADIAL DIRECTION, inch
EQUAL POTENTIAL LINES AND STREAMLINES FOR CASE I
ψ = 90%
ψ = 80%
ψ = 70%
ψ = 60%
ψ = 50%
ψ = 40%
ψ = 30%
ψ = 20%
ψ = 10%
φ = 80%
φ = 70%
φ = 60%
φ = 50%
φ = 40%
φ = 30%
φ = 20%
φ = 10%

A new scheme must therefore be devised in order to determine the true contact resistance from the information about the electrical field. The first step is to divide the bed region into increments according to the stream lines just as was done in Figure 2. In that diagram the number of increments is 10. Each increment can be represented by three lumped resistances in series, namely contact resistance at the wall electrode, bed resistance and the contact resistance at the center electrode. The resistances of all the increments are parallel to each other and the whole system can be represented by the circuit shown in Figure 3. R_{cei}, R_{bi} and R_{cwi} are, respectively, the contact resistance at the center electrode, bed resistance and contact resistance at the wall electrode in the ith increment. N is the total number of increments. Points between R_{cei} and R_{bi} (i from 1 to N) now represent the surface of the center electrode and are not at the same potential. However, as the number N increases, the surface area of the center electrode occupied by each increment, A_{ei}, becomes smaller and the electrical potential over that area gradually becomes uniform. R_{cei} is then:

$$R_{cei} = \frac{\rho_{ce}}{A_{ei}} \tag{7}$$

From the circuit shown in Figure 3 the contact resistance at the center electrode, R_{ce}, is:

$$R_{ce} = \sum_{i=1}^{N} \frac{R_{cei}}{\left(\sum_{i=1}^{N} \frac{1}{R_{cei}+R_{bi}+R_{cwi}}\right)^2 (R_{cei}+R_{bi}+R_{cwi})^2} \tag{8}$$

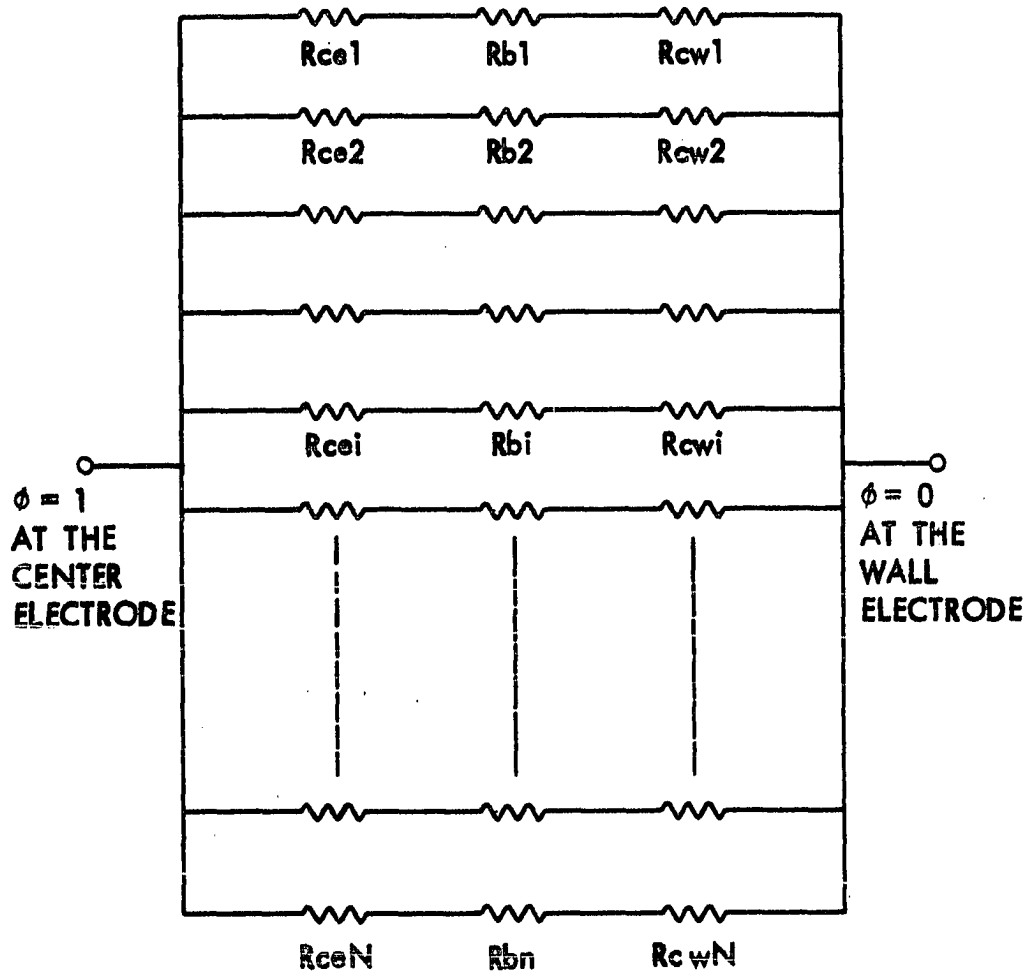

Figure 3. Simulated circuit for the system shown in Figure 1

Since

$$\frac{V_{cei}}{V_t} = \frac{R_{cei}}{R_{cei} + R_{bi} + R_{cwi}}, \qquad \frac{1}{R_t} = \sum_{i=1}^{N} \frac{1}{R_{cei} + R_{bi} + R_{cwi}} \tag{9}$$

where V_{cei} is the voltage drop over the resistance R_{cei} and R_t and V_t are the total resistance and the total voltage applied, respectively. Combining equations (7), (8) and (9) to eliminate R_{cei}, R_{bi} and R_{cwi}, equation (10) results,

$$R_{ce} = \frac{R_t^2}{\rho_{ce}} \sum_{i=1}^{N} \left(\frac{V_{cwi}}{V_t}\right)^2 A_{ei} \qquad \text{(when N is very large)} \qquad (10)$$

The same argument gives the contact resistance at the wall electrode, R_{cw}, as:

$$R_{cw} = \frac{R_t^2}{\rho_{cw}} \sum_{i=1}^{N} \left(\frac{V_{cwi}}{V_t}\right)^2 A_{wi} \qquad \text{(when N is very large)} \qquad (11)$$

where

V_{cwi} = voltage drop across the resistance R_{cwi}

A_{wi} = surface area of the wall electrode occupied by the ith increment

Dividing the applied voltage by the total current crossing any equipotential line will give the value of R_t. This together with equations (10) and (11) then enable us to calculate the contact resistances both at the center and wall electrodes. The bed resistance is the balance of the total resistance. The result of this calculation is given in Table 2 and the resistance is compared with the one calculated when the contact resistance is not considered.

The bed resistance calculated for Case I is found to be 10 times that for Case II when the contact resistances are not considered in both cases (Table 2). Since the bed resistivity assigned for the former case is also 10 times that for the latter one, the above observed result can be taken as a consequence of the linear nature of the Laplace's equation employed to describe the potential fields in both cases.

The field plots (Figure 2) provide a good indication of where heat would be generated in the bed volume of both systems. The same amount of power would be dissipated or converted into heat in each curvilinear segment of the bed because the voltage drop across and the current flow through each segment are the same. Therefore, the power dissipation would be the highest where the concentration of curvilinear segments is greatest. In both systems, practically all the heat generated in the bed volume would take place in the vicinity of the center electrode (Figure 2). In addition to that, the power could also be generated at the surface of the electrodes. As Case II showed a pair of contact resistances (Table 2) comparably larger than the bed resistance, a large release of heat at the wall and center electrodes is expected. The heat dissipated at the center electrode when added to the one generated in the immediately surrounding bed volume is quite large and may partially explain why some operating electrodes have been observed to be much hotter than the rest of the bed (1).

A SEMI-EMPIRICAL CORRELATION FOR THE BED RESISTIVITY

In this part, Bruggeman's theory for composite materials (2) will be used to predict the bed resistivity in an electrofluid bed. This extension is only for the case when the gas flowrate is less than U_{br}, the velocity at which bubbles start to rise. Before applying Bruggeman's equation (equation (3)), his derivation must be examined more closely to find its range of application. For Bruggeman's theory to apply the following three conditions have to be met:

1. the dispersion of particles must be completely random,
2. the dispersed particles need to be spherical in shape, and
3. the continuous medium must be conductive.

If the gas phase and the solid particles of the electrofluid bed correspond respectively to the continuous medium and the dispersed phase of a composite material, the three requirements are not met. First, the bed particles are not a completely random dispersion when the gas velocity is smaller than U_{br}. Furthermore, most of the materials processed in the electrofluid bed are not spherical particles. Finally, if the main mechanism for current flow is along conducting chains, the gas phase is nonconducting. Therefore, equation (3) must be modified to fit this situation.

As the gas starts to flow through a settled bed, most of the bed is undisturbed and only a few particles begin to vibrate or circulate in some region not very far from their original positions. As the gas flowrate gradually increases, both the number of disturbed particles and their range of movement increase. Finally, the particles become

completely free to move and the bed expands significantly and now bubbles may even rise through it. If the settled bed is taken as the basic structure of an imaginary continuous medium, then areas occupied by the circulating particles can be thought of as particles dispersed in an imaginary continuous medium. These fictitious particles are all nonconducting because the corresponding real bed particles are in motion and not in contact with adjacent particles; in other words, the conducting chains are interrupted there. The volume fraction of nonconducting particles is unknown, but is simply assumed to be a function of the relative fluidization velocity which is the ratio between the fluidization velocity and the one at minimum fluidization condition. This semi-empirical model is now compatible with the conditions required for the application of Bruggeman's equation, except the second one. However, experimental evidence indicates that as long as the dispersed particles in a composite material are nonconductive, particle shape usually does not have an appreciable affect on the effective conductivity (35).

Since the settled bed is taken as the basic structure of the imaginary continuous medium in the derivation of the equation for the bed resistivity, its fundamental character needs to be pursued in more detail. One character that is of particular interest is the average volume of the settled bed shared by each particle. This can be found from the following relation:

$$1 - \epsilon_s = nV_p/V_{bs} \tag{12}$$

or

$$V_{bs}/n = V_p/(1 - \epsilon_s) \tag{13}$$

where

ϵ_s = voidage of the settled bed

V_p = volume of each particle

n = total number of particles in the bed

V_{bs} = volume of settled bed

By denoting f_d as the fraction of undisturbed particles, the volume fraction of the nonconducting fictitious particles f can be expressed as:

$$f = \frac{V_b - nf_d(V_{bs}/n)}{V_b} = 1 - \frac{nf_dV_p}{V_b(1 - \epsilon_s)} \tag{14}$$

However, since

$$1 - \epsilon = nV_p/V_b$$

equation (14) can be rewritten as:

$$f = 1 - (\frac{1 - \epsilon}{1 - \epsilon_s})f_d \tag{15}$$

where ϵ and V_b are respectively the voidage and bed volume at a given flowrate. Using Bruggeman's result for the case of a nonconducting dispersed phase, then

$$K_m/K_c = \left[\frac{(1 - \epsilon)f_d}{1 - \epsilon_s}\right]^{3/2} \tag{16}$$

where

K_m = bed conductivity or the inverse of bed resistivity

K_c = conductivity of the imaginary continuous medium

Although the imaginary continuous medium always has the basic structure of the settled bed for the entire range of gas flowrates considered, the load imposed on it varies as the gas flowrate increases. For an electrofluid bed, the load is the bed weight minus the pressure drop through the bed at the given gas flowrate. As noted by Holm (16), the resistance due to the body contact of particles is proportional to the load imposed raised to the negative 1/3 power. Therefore, K_c of equation (16) is expected to be a function of the pressure drop such as:

$$K_c = K_{cs}\left(\frac{(\Delta P)_{eq} - \Delta P}{(\Delta P)_{eq} f_d}\right)^{1/3} \tag{17}$$

where

K_{cs} = conductivity of the settled bed

$(\Delta P)_{eq}$ = bed weight divided by the cross-sectional area of the bed column

ΔP = pressure drop through the bed

Since the resistivity is just the inverse of conductivity, equation (16) combined with equation (17) gives the final semi-empirical correlation for the bed resistivity:

$$\rho_b = \rho_{cs}\left(1 - \frac{\Delta P}{(\Delta P)_{eq}}\right)^{-1/3}\left(\frac{1 - \epsilon}{1 - \epsilon_s}\right)^{-3/2} f_d^{-7/6} \tag{18}$$

Using the fact that

$$\frac{L_s}{L} = \frac{1 - \epsilon}{1 - \epsilon_s}\,, \tag{19}$$

rearrangement of equation (18) gives

$$f_d = \left(\frac{\rho_{cs}}{\rho_b}\right)^{6/7}\left(\frac{(\Delta P)_{eq}}{(\Delta P)_{eq} - \Delta P}\right)^{2/7}\left(\frac{L}{L_s}\right)^{9/7} \tag{20}$$

where L represents the bed height and the subscript s denotes the settled bed. All the terms on the right side of equation (20) can be measured experimentally to determine the value of f_d at different gas flowrates.

EXPERIMENTAL MEASUREMENT OF BED AND CONTACT RESISTANCES

To justify the semi-empirical correlation presented in the preceding section as well as to collect information about contact resistances, bed resistivities and contact resistances were determined experimentally in a concentric electrofluid bed at room temperature and atmospheric pressure. The gas velocities used covered the whole range of fluidization conditions starting from the settled bed and ending at a fully fluidized condition. In all runs nitrogen served as the fluidizing gas and the current was set between 0.29 and 1.16 amperes to insure a small current density in the bed. Such operating conditions should prevent most of the arcing in the electrofluid bed and conducting chains should prevail as the path for current flow.

Five probes were inserted into the bed to trace out the potential profile between the center and wall electrodes. From this both the bed resistivities and contact resistances were calculated. Two bed materials, calcined coke and graphite, and four types of center electrode materials (brass, graphite, stainless steel and silicon carbide) were tried. Most of the rods were 1 inch in diameter, except the brass rod where 1/2 and 1-1/2 inch diameter rods were also tried.

Apparatus

The apparatus used to measure the electrical properties inside an electrofluid bed consisted of three parts;

1. a nitrogen gas recycle system,
2. a fluidization column,

3. the electrical instruments which measured and recorded all the voltage drop readings.

A flow sheet of the nitrogen recycle system is shown in Figure 4. The system was designed to supply the gas for fluidization and then to recirculate the gas to reduce the cost of operation. Before start-up of the system, the gas holder was first charged with nitrogen from a gas tank. The gas holder had a counterbalance weight so that the gas in it was automatically kept at one atmosphere all the time. Once the system was started, the gas entered a compressor. The gas left the compressor at a pressure of 15 psig and immediately went through a felt-element oil trap where small oil droplets introduced in the compression stage were removed. This oil-free gas then passed through a finned-tube cooler which removed the heat generated from the compression of the gas. A silica gel dryer was placed after the cooler; when the gas passed through the dryer, moisture in the nitrogen was absorbed. Following the dryer was a bypass line for returning the excess gas not needed for fluidization to the gas holder. The flowrate of the gas to the fluidization column was controlled by adjusting a bypass control valve and was measured by a gas rotameter. Any fine bed particles elutriated in the exit gas from the fluidization column were trapped in a filter and the cleaned gas was then returned to the gas holder.

The fluidization column, shown in Figure 5, was a 6 inch I.D. Plexiglass tube. The 4.5 foot long upper section of the column was mainly for preventing entrainment of bed particles, while the lower section, 36 inches in length, was the test column and contained the bed. A porous plate at the bottom of the column served as the gas

Figure 4. Flow sheet of gas recycle system

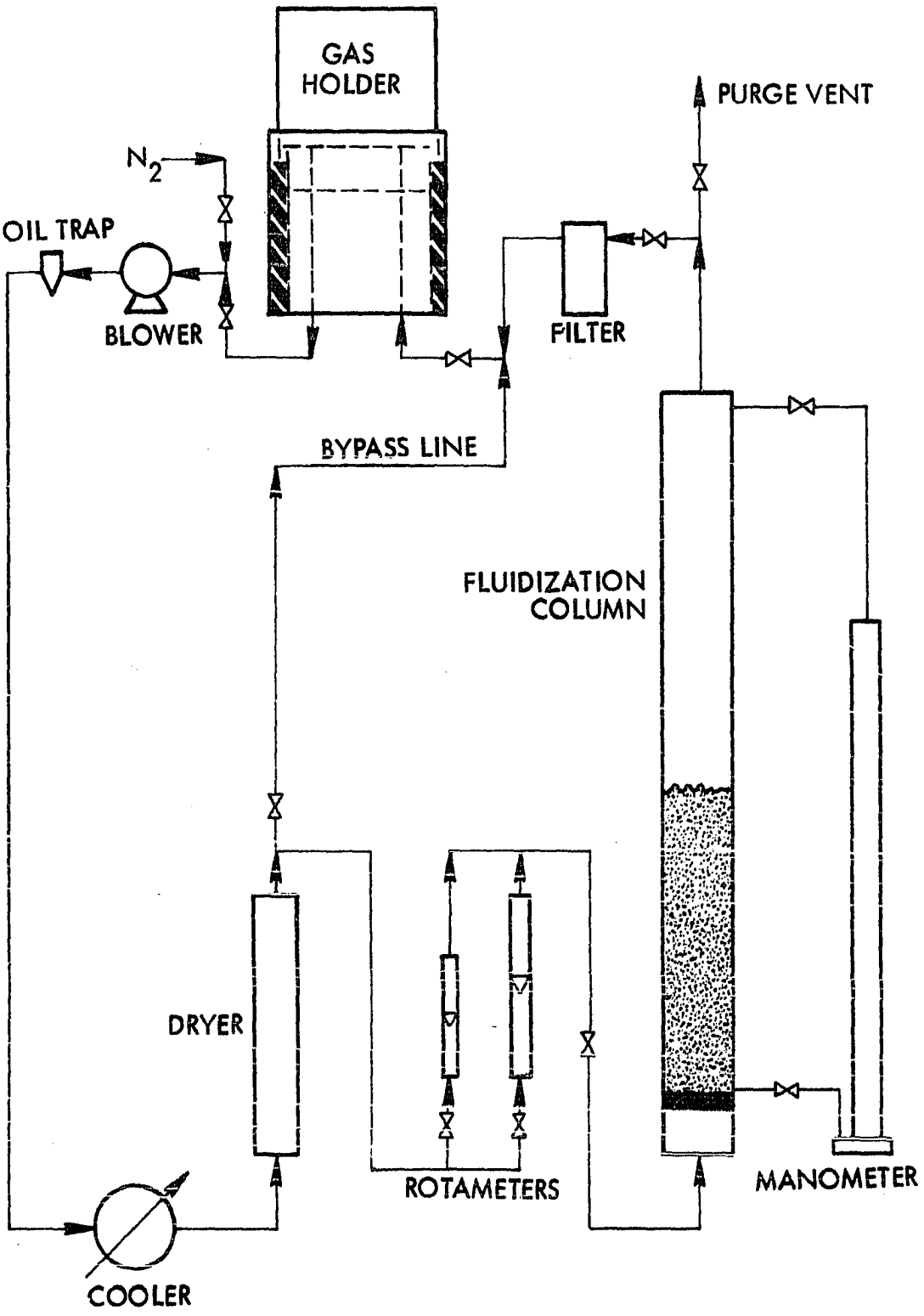
GAS
HOLDER
PURGE VENT
N_2
OIL TRAP
BLOWER
FILTER
BYPASS LINE
FLUIDIZATION
COLUMN
DRYER
ROTAMETERS
MANOMETER
COOLER

Figure 5. Schematic representation of fluidization column

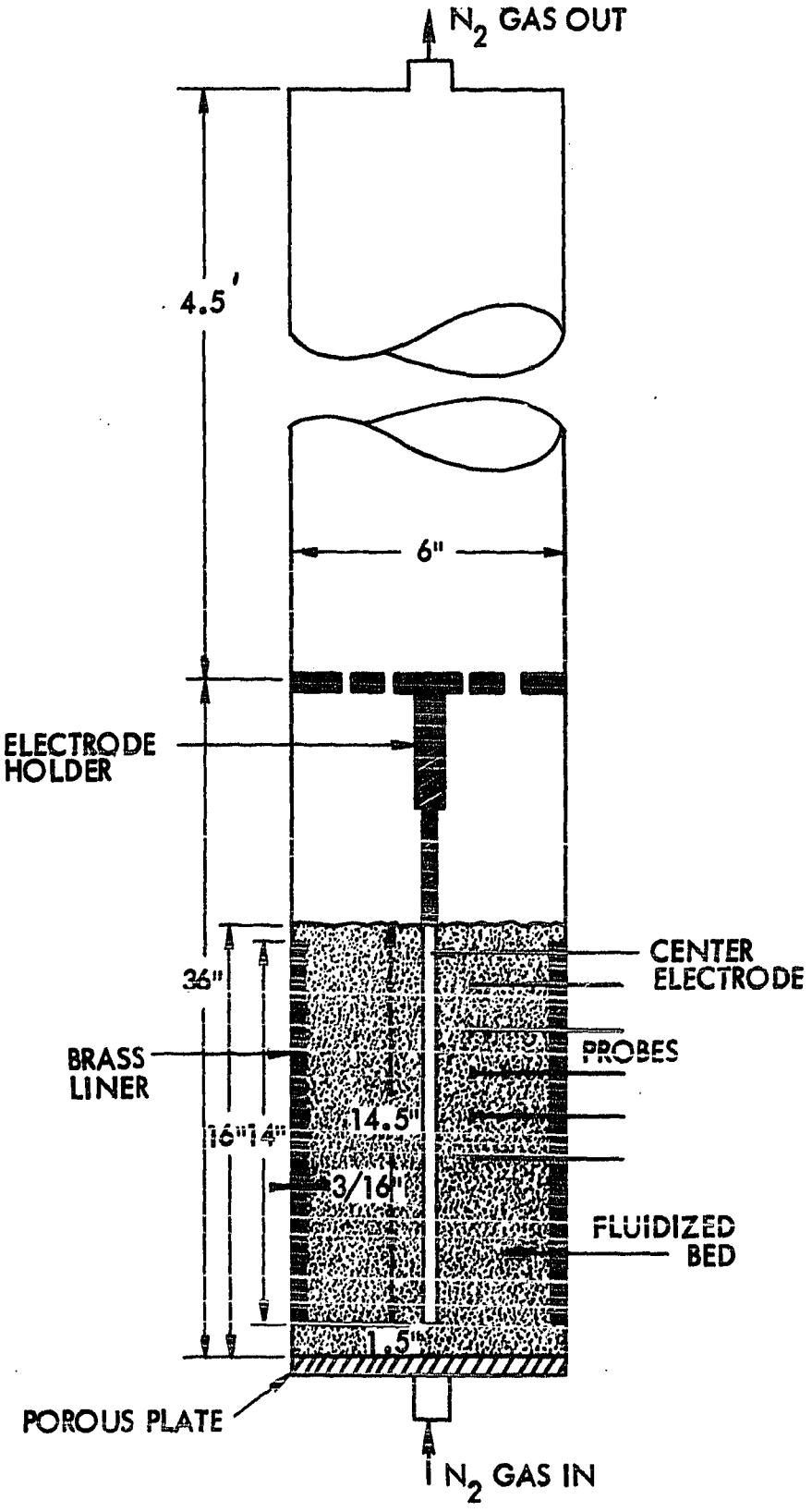
N_2 GAS OUT
4.5'
6"
ELECTRODE HOLDER
CENTER ELECTRODE
PROBES
36"
BRASS LINER
14.5"
16"14"
3/16"
FLUIDIZED BED
1.5"
POROUS PLATE
N_2 GAS IN

distributor. The center electrode was positioned by an electrode holder which sat on top of the test column. All the center electrode rods used were 14.5 inches long with their tips insulated and were 1.5 inches from the gas distributor. The electrode holder was a brass plate; a number of holes were drilled through the plate so that the nitrogen could pass through. A brass liner was cemented to the inner wall of the test column and served as the wall electrode. This liner was 14 inches high and 3/16 inches thick with its bottom rim 1-1/2 inches from the gas distributor. The pressure drop through the bed was measured by a manometer connected by two plastic tubes to the bottom and top of the test column.

Five probes were inserted into the bed through five small holes drilled in the test column wall and the brass liner. They were located 6.83, 8.00, 9.16, 10.33 and 11.50 inches above the gas distributor. These probes could be moved radially to the desired position between the center and wall electrodes. Each of the five probes were identically constructed and their basic construction is shown in Figure 6. The probes were a 1/16-inch diameter brass rod with a 3/16-inch diameter brass disk attached to the tip of the rod. The surface of the probe was insulated, except for the disk which was added to achieve a better contact between the bed and the probe tip.

Shown in Figure 7 is the arrangement of the electrical circuit and the instruments. A current regulator coupled with a 0-75 volt D.C. power supply was used to establish a constant current flow through the bed. The current was then measured by recording the voltage drop

Figure 6. Probe used to measure voltage profile in a fluidized bed

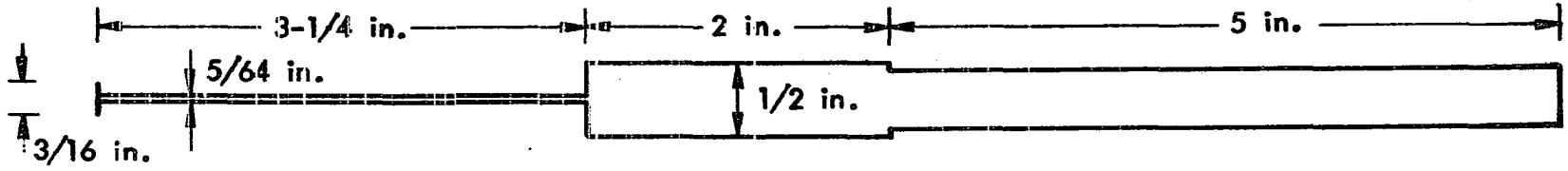
3-1/4 in.
2 in.
5 in.
5/64 in.
1/2 in.
3/16 in.

Figure 7. Electrical circuit used to measure bed and contact resistances

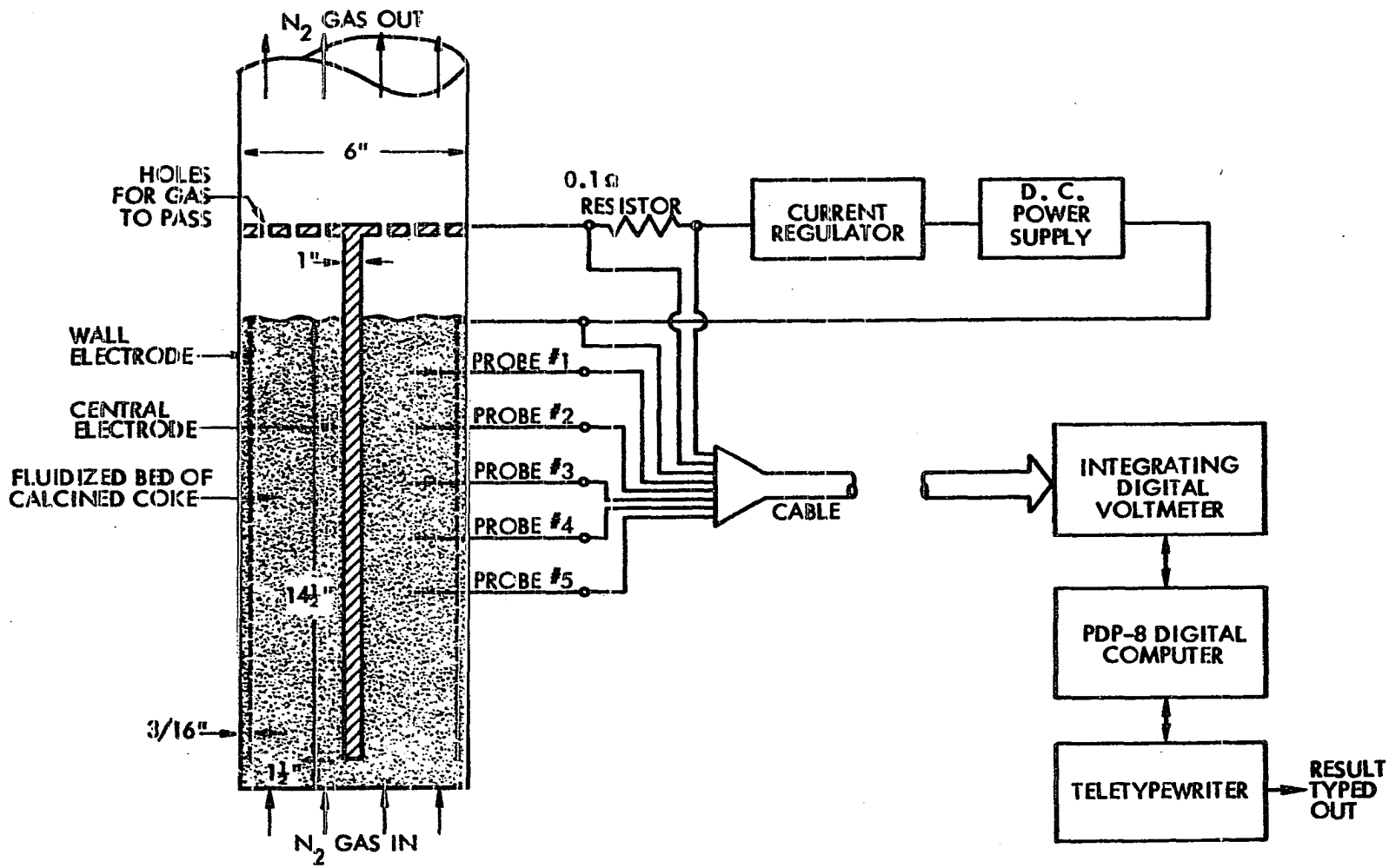
N_2 GAS OUT
6"
HOLES FOR GAS TO PASS
1"
0.1 Ω RESISTOR
CURRENT REGULATOR
D. C. POWER SUPPLY
WALL ELECTRODE
CENTRAL ELECTRODE
FLUIDIZED BED OF CALCINED COKE
PROBE #1
PROBE #2
PROBE #3
PROBE #4
PROBE #5
CABLE
14½"
3/16"
1½"
N_2 GAS IN
INTEGRATING DIGITAL VOLTMETER
PDP-8 DIGITAL COMPUTER
TELETYPEWRITER
RESULT TYPED OUT

across a 0.1 ohm shunt in series with the wall and center electrodes. Nine electrical wires were hooked to the five probes, wall electrode, center electrode and both ends of the shunt. All these wires were then contained in a single cable that ran between the apparatus and the computer room. An integrating digital voltmeter capable of averaging the voltage drop readings between any two of the nine wires over a given time period was located in the computer room and was connected to a PDP-8 digital computer. Choice of the wires to be read was made by the computer. Voltage drop readings of interest were the ones between (1) the probe and wall electrode, (2) the probe and the center electrode, (3) the wall and center electrodes and (4) the two ends of the shunt. All these measured values were typed out by a teletypewriter associated with the computer.

Experimental Procedure

To start a run, a given bed material was charged to the test column until the resulting settled bed reached a height of 16 inches. The length of each probe extending outside the column was measured when the disk at the tip of the probe touched the center electrode. This length was referred to as the zero position of that probe. When the probe was moved to a new position, its length outside the column changed. Comparing this with the zero position revealed the distance between the probe and the center electrode.

In measuring the voltage drops, all five probes were fixed at the same position. Seven probe positions were chosen so as to trace

out the potential profile. The positions were 0.125, 0.25, 0.375, 0.625, 0.875, 1.125 and 1.625 inches from the surface of the center electrode. After the probes were set at a given position, the whole column was sealed and the nitrogen was circulated to the bed. The gas flowrate was first set at the largest reading on the rotameter; for the three beds investigated, this gave a fully fluidized condition. The D.C. power supply and the current regulator were then turned on and set to give a steady current flow through the bed. A small program stored in the PDP-8 digital computer was used to control the integrating digital voltmeter so that it took in turn each of the voltage drop readings of interest averaged over a ten-second period. Once this was accomplished, the bed height was measured and the pressure drop was read from the manometer. The gas flowrate was then changed to a lower rotameter reading and the above procedure was repeated. In total, more than 15 gas flowrates were tried before the gas velocity was reduced to zero. After that, a new probe position was tried. When all seven probe positions had been tried, the data were used to determine the dependency of contact resistance and bed resistivity on gas flowrate for the given combination of bed material and center electrode. New combinations were examined in exactly the same way.

Method of Analyzing the Data

In this section, the data from one particular run will be used as an example to exhibit the method of analyzing the experimental results. In the run chosen, a 1-inch diameter brass center electrode

was immersed in a calcined coke bed (-65+80 mesh) and the current was set at 0.58 amperes. Shown in Figures 8, 9 and 10 are the relationships between the gas flowrate and pressure drop across the bed, bed height, and the voltage drop between the center and wall electrodes. Information given in these diagrams will be used later for the semi-empirical correlation as proposed earlier for the bed resistivity. From Figure 8, the minimum fluidization velocity was found to be at a gas flowrate of 0.76 SCFM. Given in Figures 11 through 17 are a series of plots of the voltage drop between the probe and wall electrode as a function of gas flowrate. Data points shown in these plots represent the average of the values measured by the five probes; the voltage drop readings given from an individual probe deviated from the mean value by less than 10%.

As indicated by Yuan (51), the experimental setup in the test column resembled the 14.5-inch ideal concentric system shown in Figure 18(b). The voltage distribution for such an electrode measurement is

$$V = V_b + (V_a - V_b)(\ln b - \ln r)/(\ln b - \ln a) \qquad (21)$$

where

V = voltage drop between probe and wall electrode

V_a = voltage drop between center and wall electrodes, with the voltage drop due to the contact resistance at the center electrode excluded

V_b = voltage drop due to the contact resistance at the wall electrode

Figure 8. Effect of gas flowrate on bed resistivity and pressure drop for 1-inch diameter center electrode in the -65+80 mesh calcined coke bed at current of 0.58 amperes (Runs 2, 3, 4 and 5)

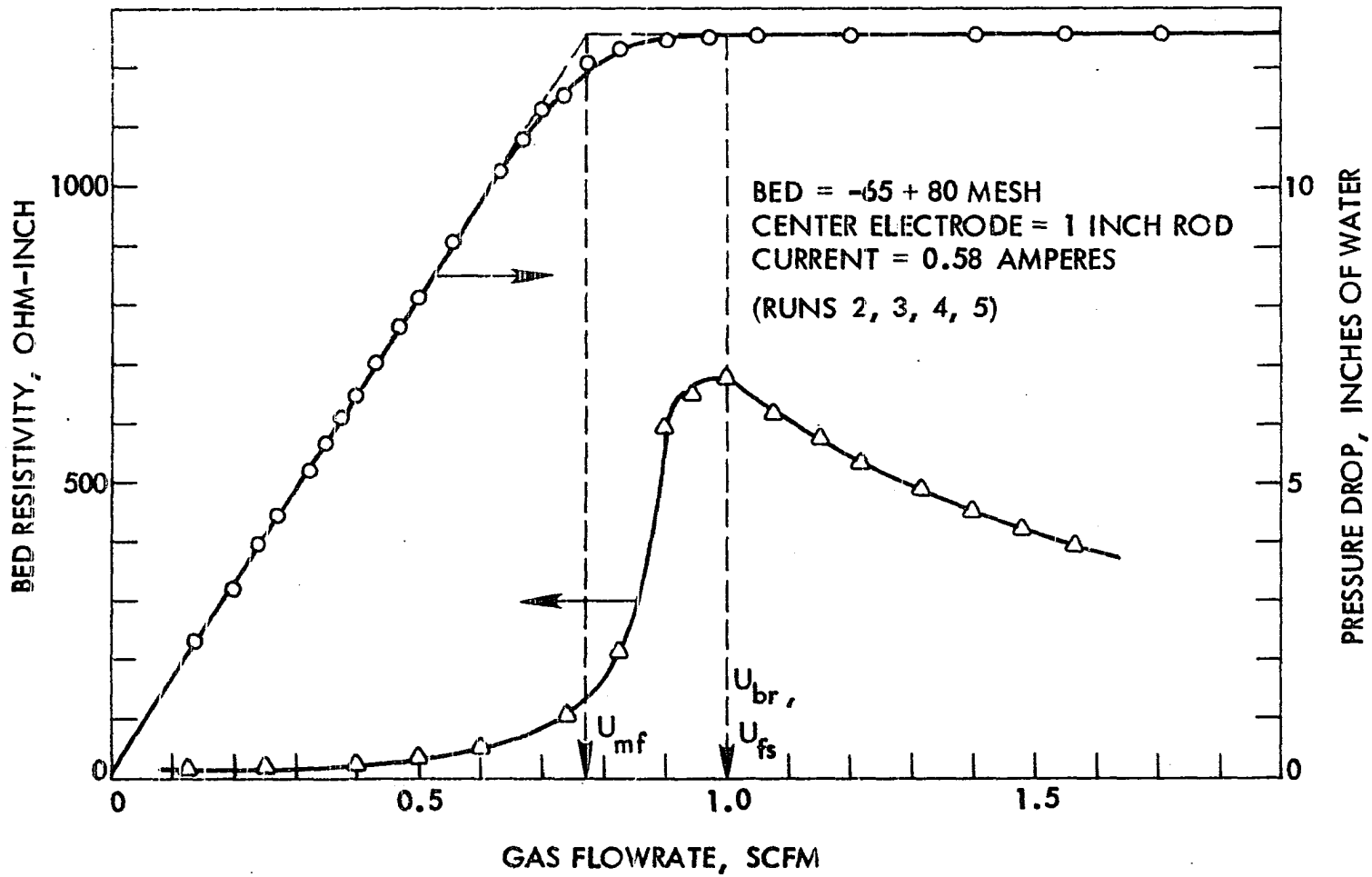
BED RESISTIVITY, OHM-INCH
PRESSURE DROP, INCHES OF WATER
BED = -65 + 80 MESH
CENTER ELECTRODE = 1 INCH ROD
CURRENT = 0.58 AMPERES
(RUNS 2, 3, 4, 5)
1000
500
0
10
5
0
0
0.5
1.0
1.5
U_{mf}
U_{br} ,
U_{fs}
GAS FLOWRATE, SCFM

Figure 9. Effect of gas flowrate on bed height.

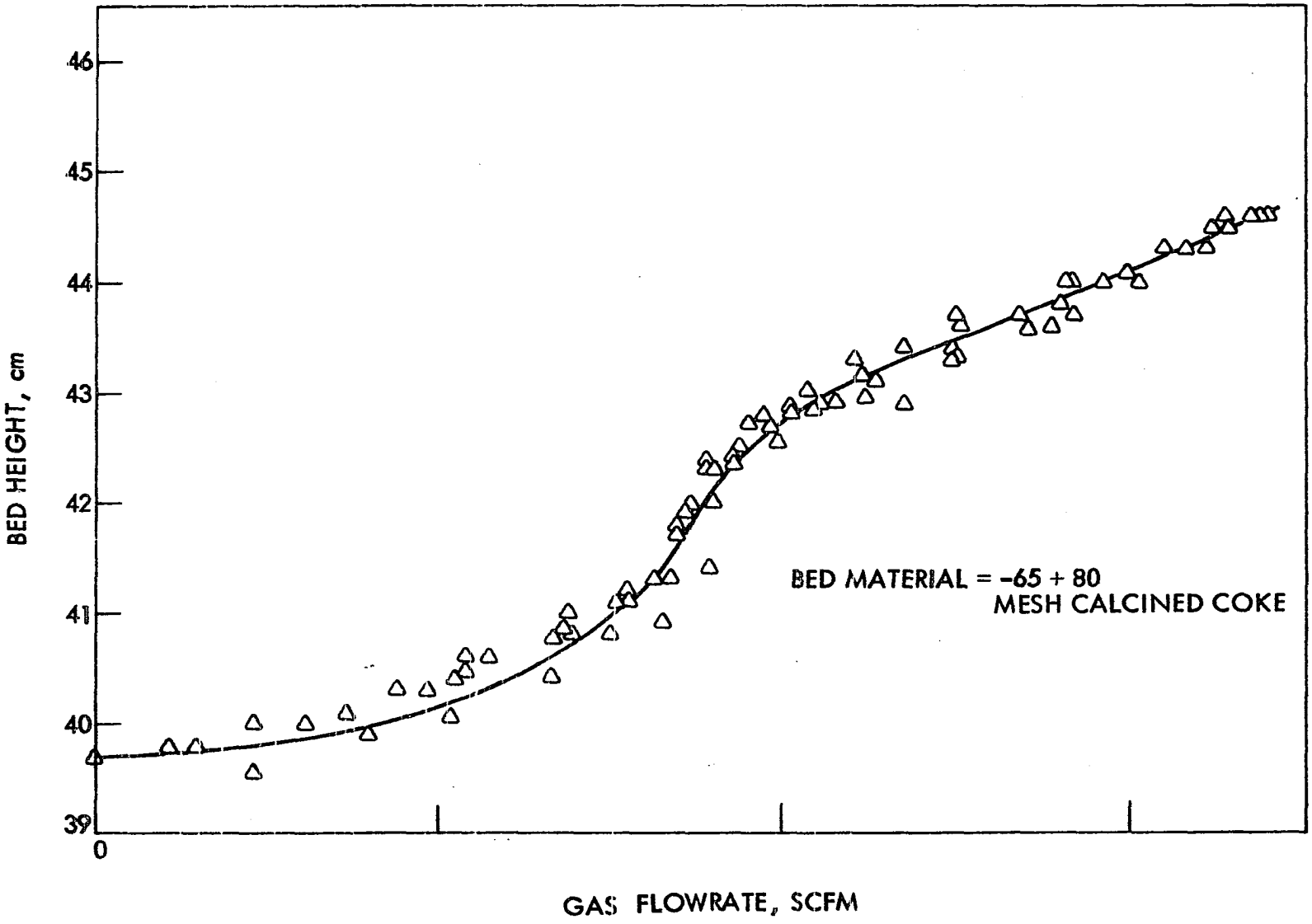
BED HEIGHT, cm
46
45
44
43
42
41
40
39
0
GAS FLOWRATE, SCFM
BED MATERIAL = -65 + 80
MESH CALCINED COKE

Figure 10. Comparison of voltage drop caused by bed to total voltage drop between electrodes

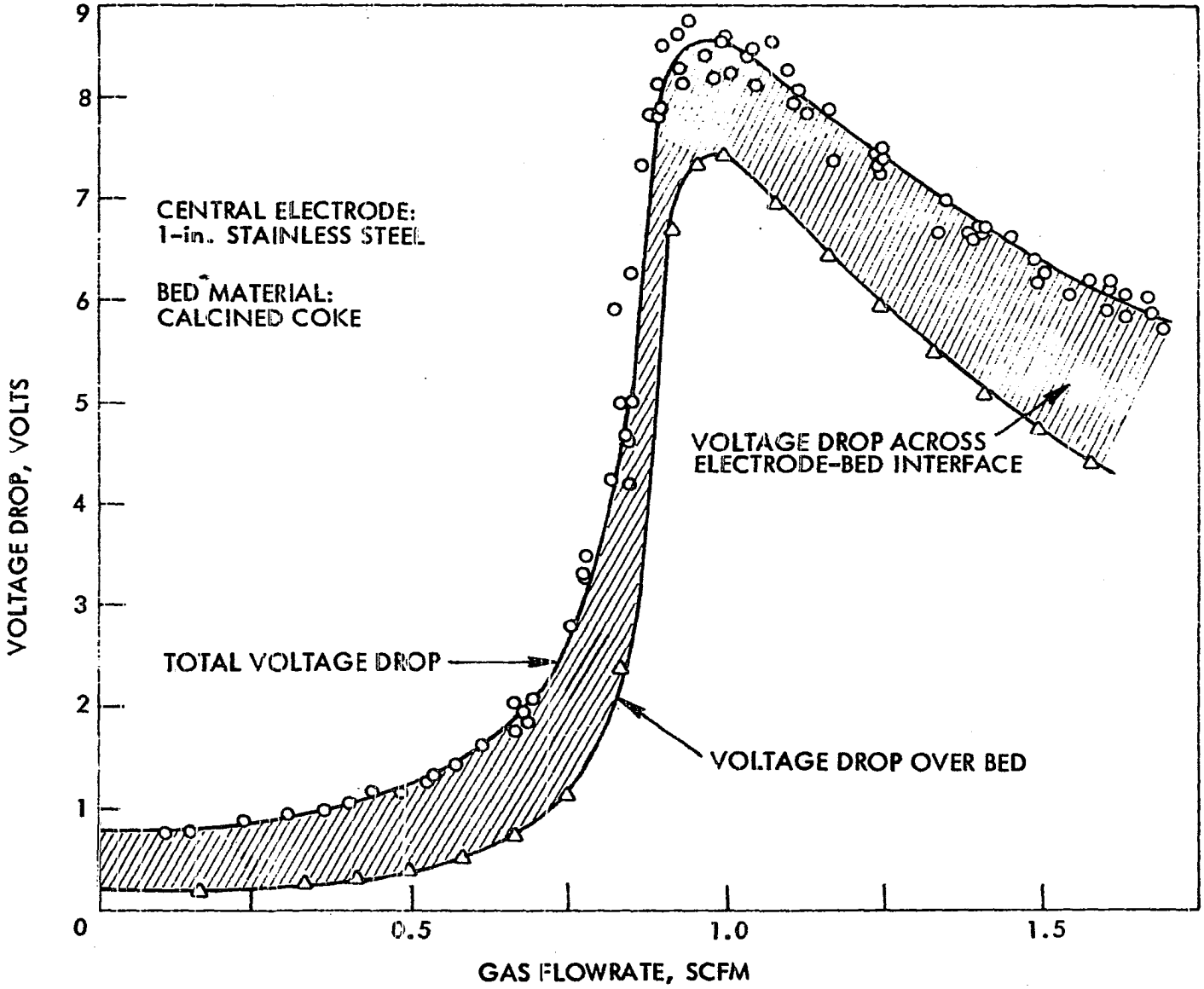
VOLTAGE DROP, VOLTS
GAS FLOWRATE, SCFM
CENTRAL ELECTRODE:
1-in. STAINLESS STEEL
BED MATERIAL:
CALCINED COKE
TOTAL VOLTAGE DROP
VOLTAGE DROP ACROSS
ELECTRODE-BED INTERFACE
VOLTAGE DROP OVER BED
0
1
2
3
4
5
6
7
8
9
0.5
1.0
1.5

Figure 11. Voltage drop between probe and wall electrode as a function of gas flowrate at r = 0.625 inches

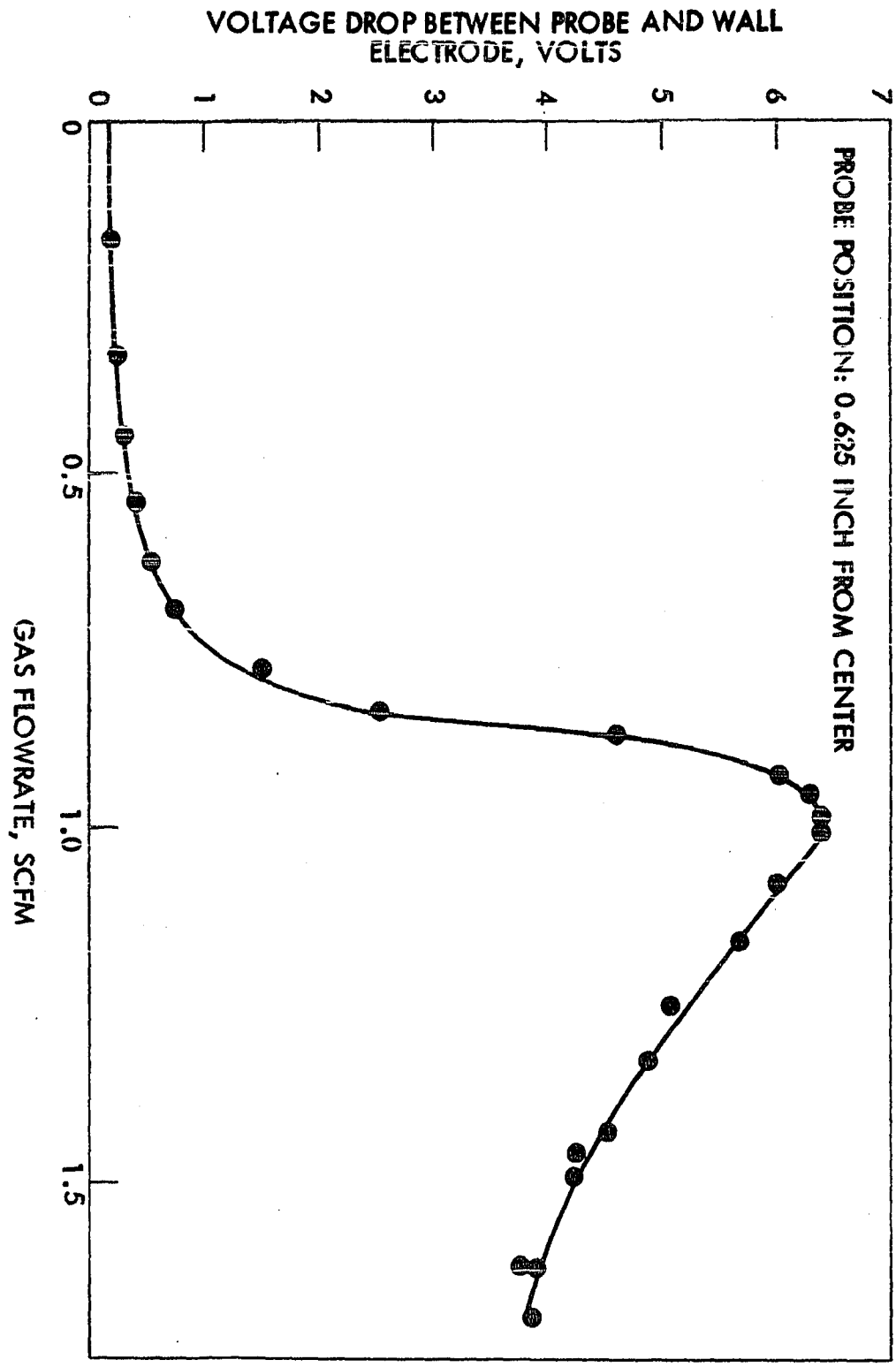
VOLTAGE DROP BETWEEN PROBE AND WALL ELECTRODE, VOLTS
0
1
2
3
4
5
6
7
PROBE POSITION: 0.625 INCH FROM CENTER
0
0.5
1.0
1.5
GAS FLOWRATE, SCFM

Figure 12. Voltage drop between probe and wall electrode as a function of gas flowrate at r = 0.75 inches

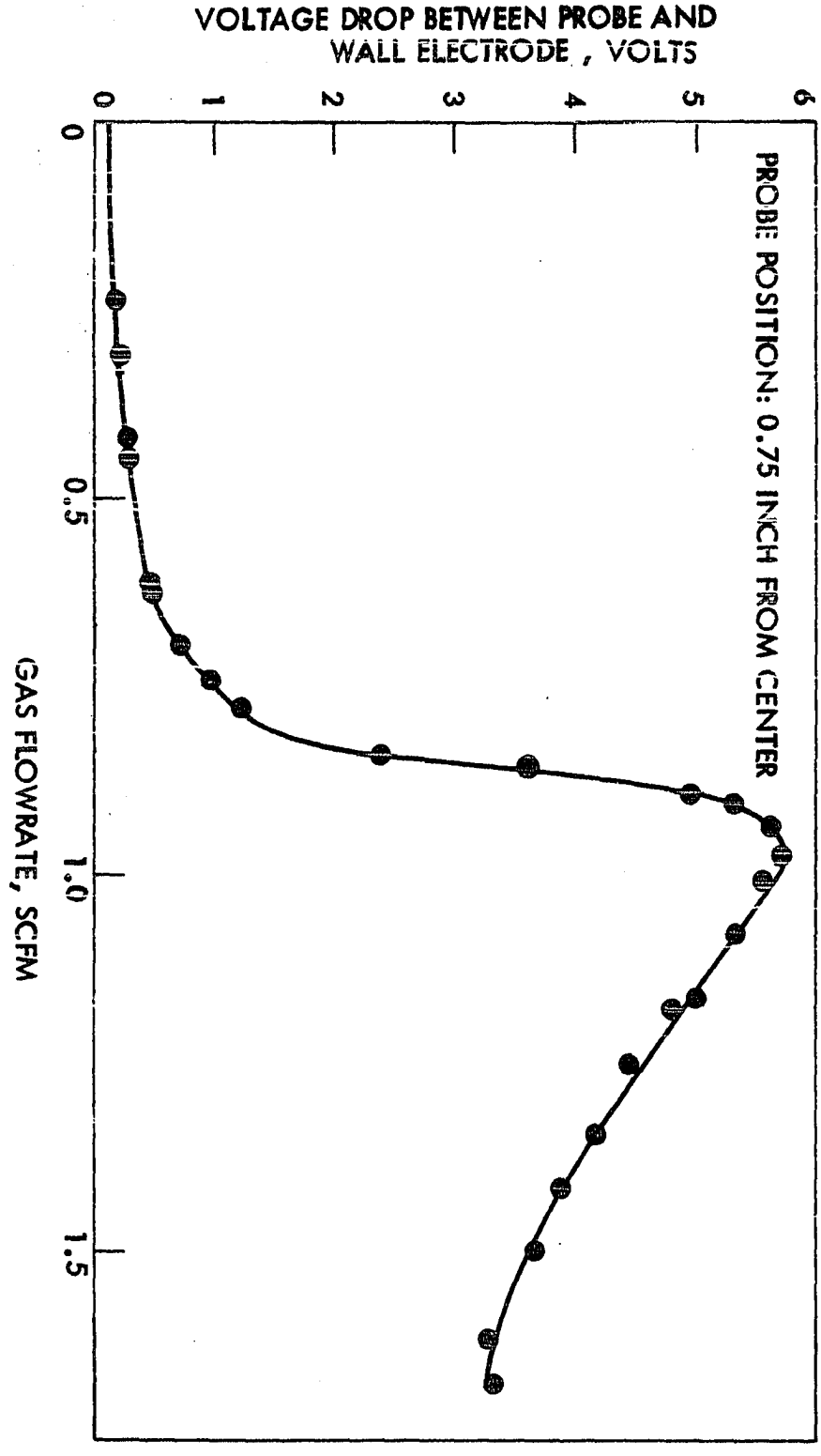
VOLTAGE DROP BETWEEN PROBE AND WALL ELECTRODE , VOLTS
0
1
2
3
4
5
6
PROBE POSITION: 0.75 INCH FROM CENTER
0
0.5
1.0
1.5
GAS FLOWRATE, SCFM

Figure 13. Voltage drop between probe and wall electrode as a function of gas flowrate at r = 0.875 inches

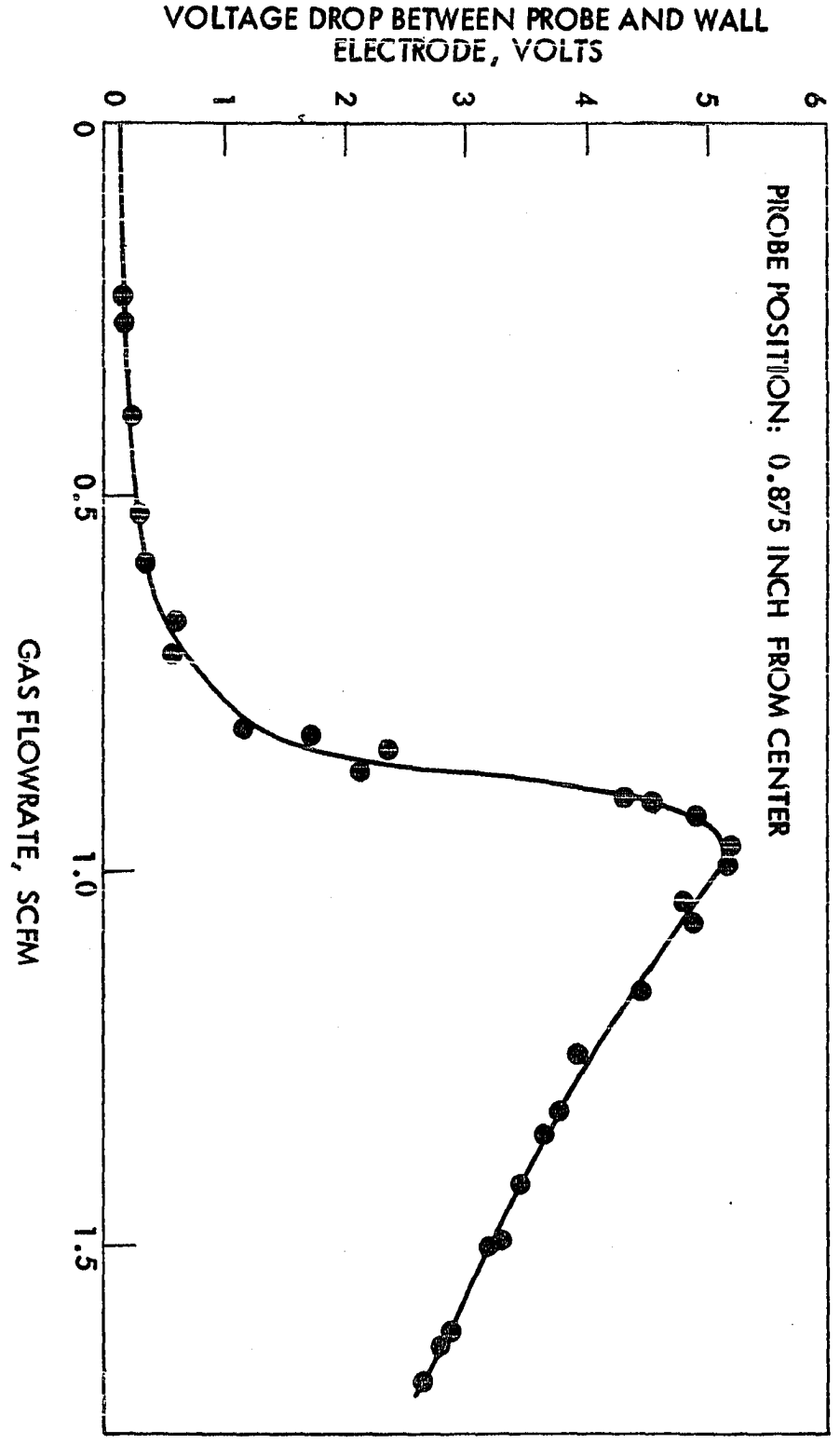
VOLTAGE DROP BETWEEN PROBE AND WALL ELECTRODE, VOLTS
0
1
2
3
4
5
6
PROBE POSITION: 0.875 INCH FROM CENTER
0
0.5
1.0
1.5
GAS FLOWRATE, SCFM

Figure 14. Voltage drop between probe and wall electrode as a function of gas flowrate at r = 1.125 inches

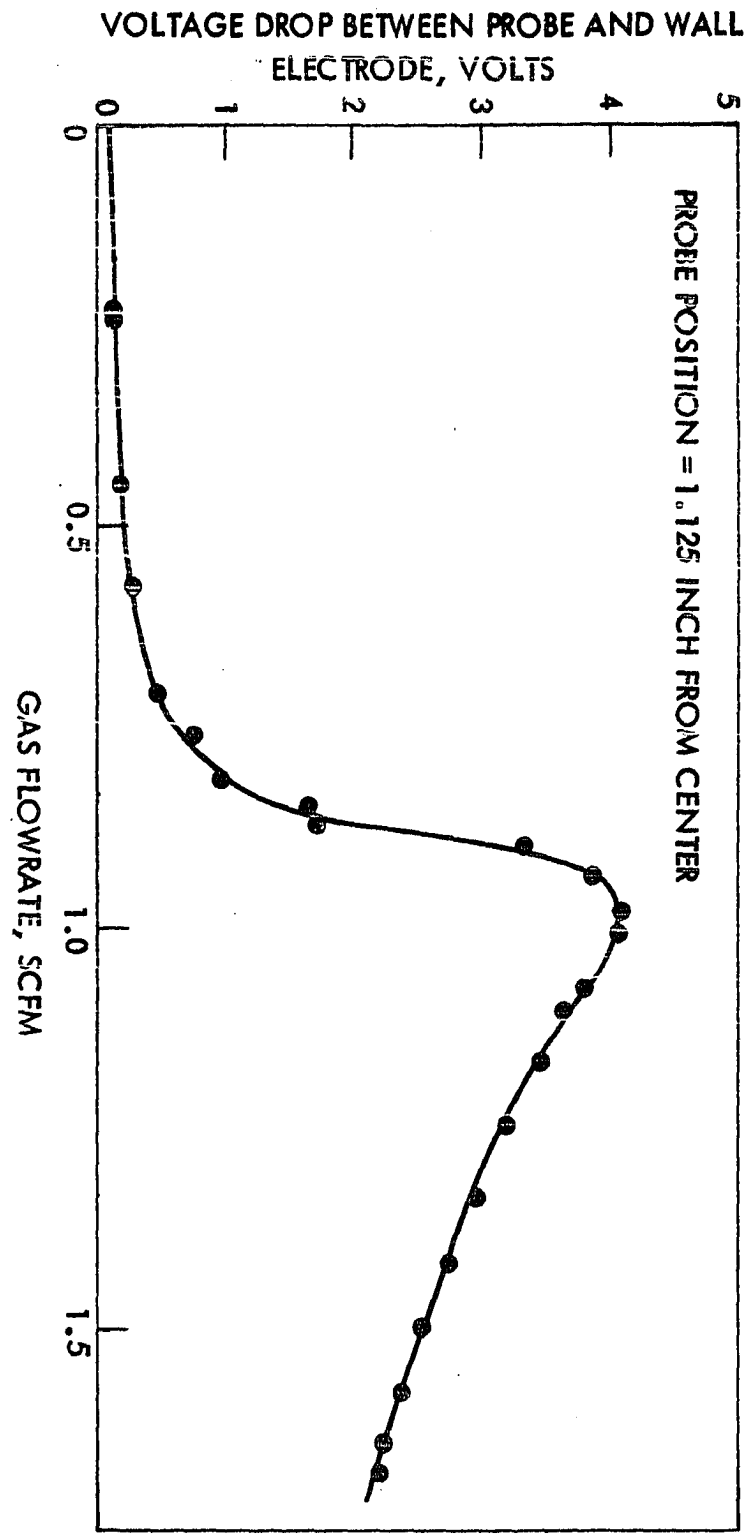
VOLTAGE DROP BETWEEN PROBE AND WALL ELECTRODE, VOLTS
0
1
2
3
4
5
PROBE POSITION = 1.125 INCH FROM CENTER
0
0.5
1.0
1.5
GAS FLOWRATE, SCFM

Figure 15. Voltage drop between probe and wall electrode as a function of gas flowrate at r = 1.375 inches

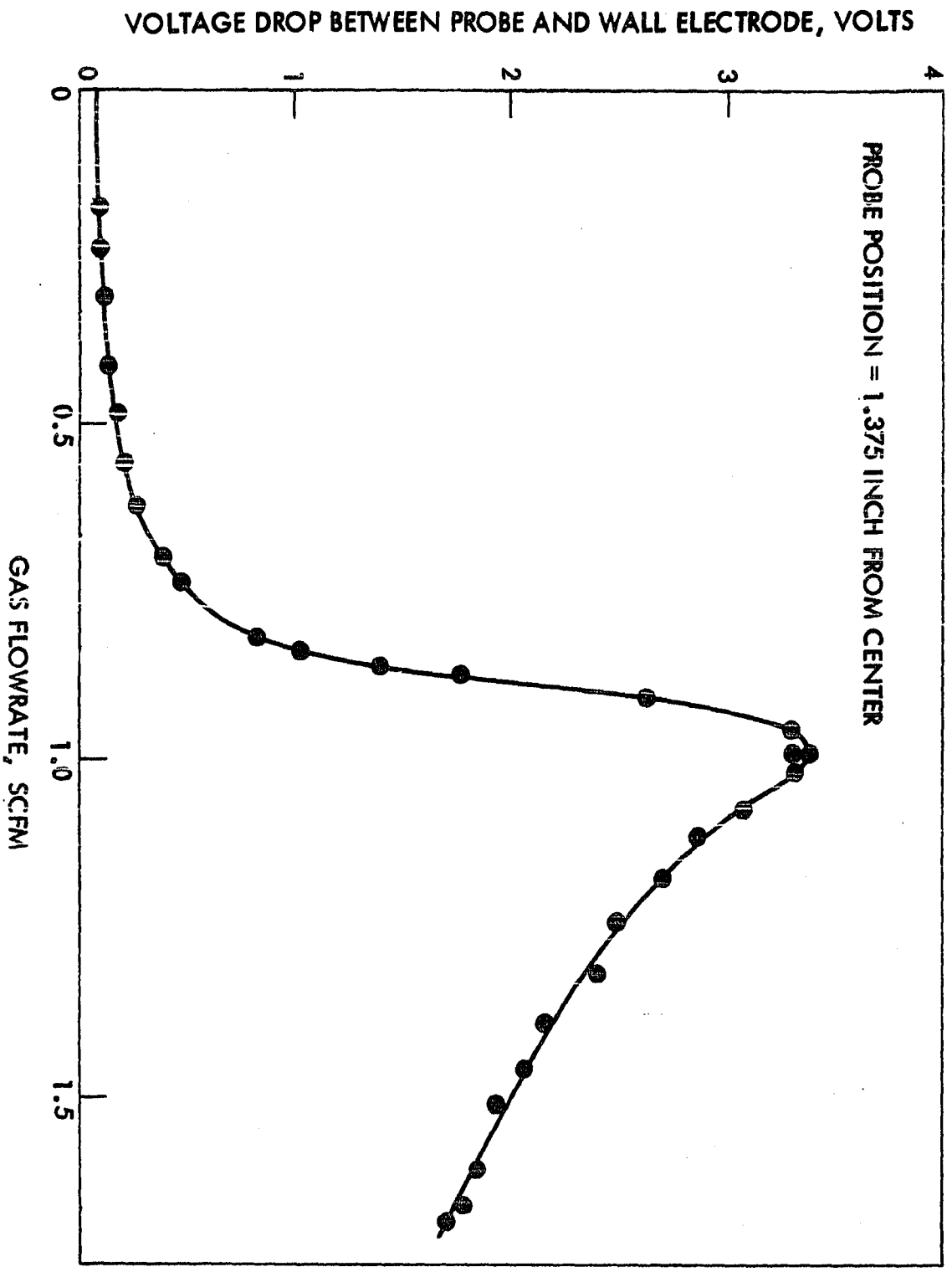
VOLTAGE DROP BETWEEN PROBE AND WALL ELECTRODE, VOLTS
0
1
2
3
4
PROBE POSITION = 1.375 INCH FROM CENTER
GAS FLOWRATE, SCFM
0
0.5
1.0
1.5

Figure 16. Voltage drop between probe and wall electrode as a function of gas flowrate at r = 1.625 inches

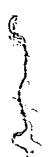

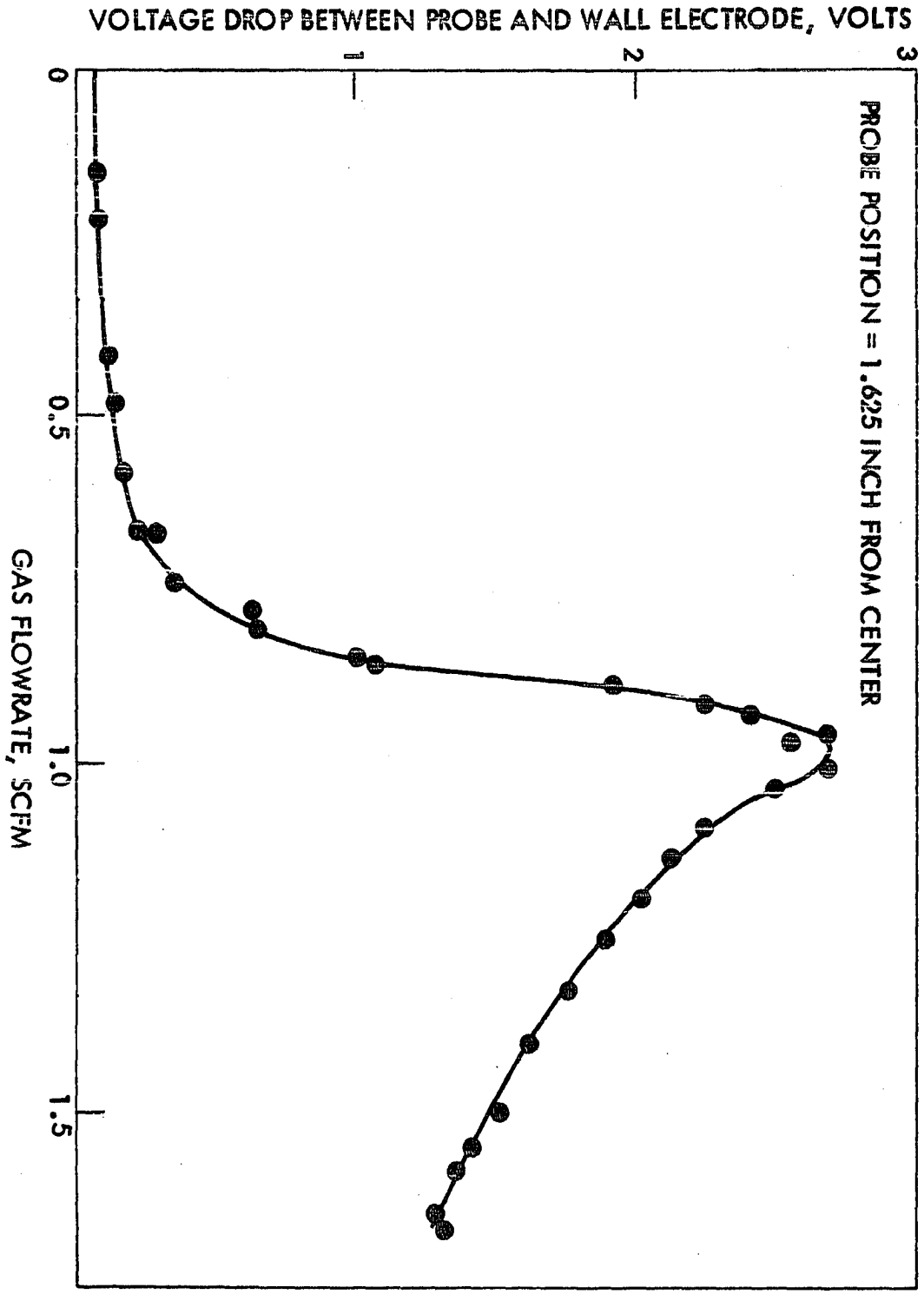
VOLTAGE DROP BETWEEN PROBE AND WALL ELECTRODE, VOLTS
0
1
2
3
PROBE POSITION = 1.625 INCH FROM CENTER
GAS FLOWRATE, SCFM
0
0.5
1.0
1.5

Figure 17. Voltage drop between probe and wall electrode as a function of gas flowrate at r = 2.125 inches

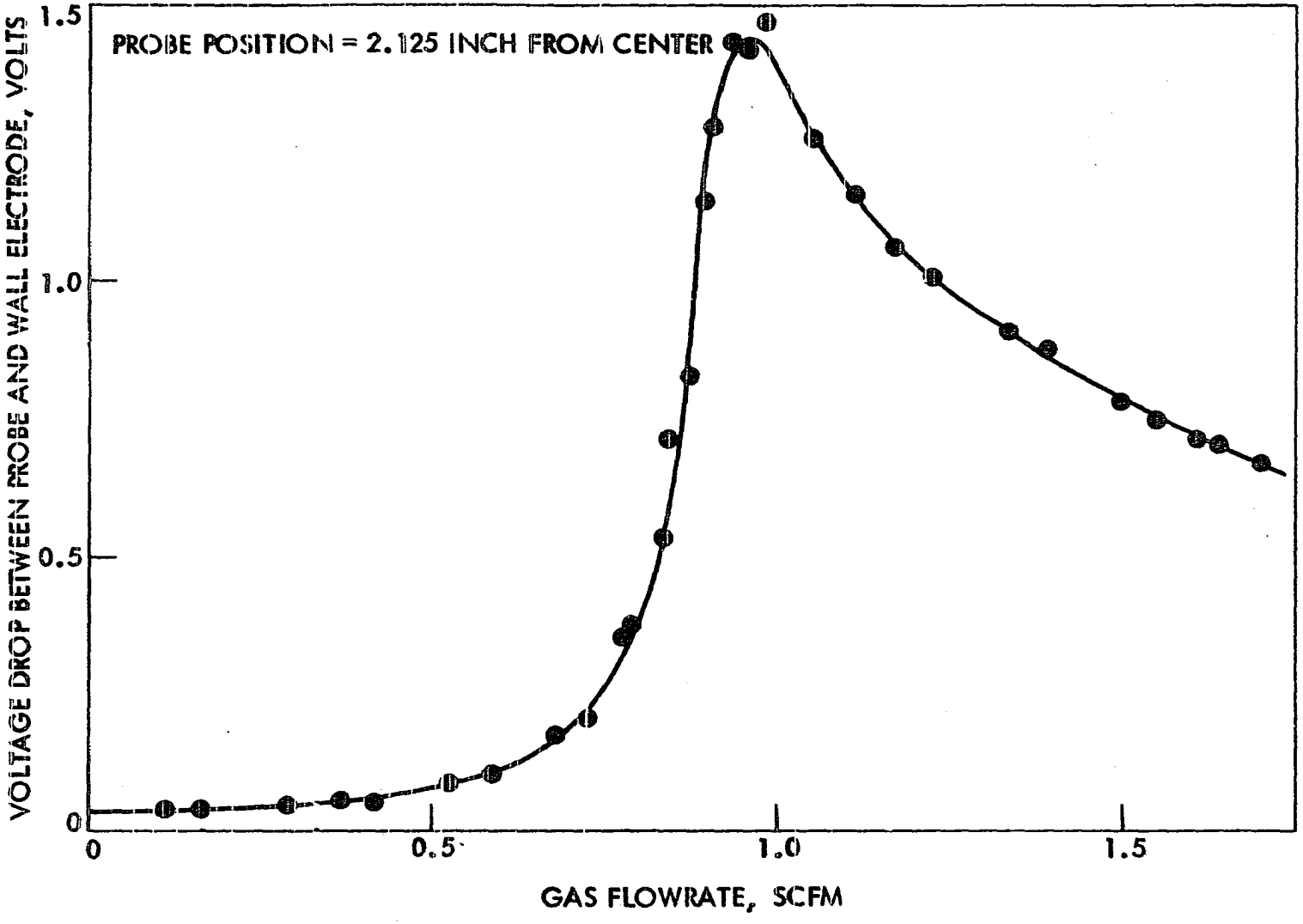
PROBE POSITION = 2.125 INCH FROM CENTER
VOLTAGE DROP BETWEEN PROBE AND WALL ELECTRODE, VOLTS
1.5
1.0
0.5
0
0
0.5
1.0
1.5
GAS FLOWRATE, SCFM

Figure 18. Bed geometry

(a) Actual

(b) Idealized

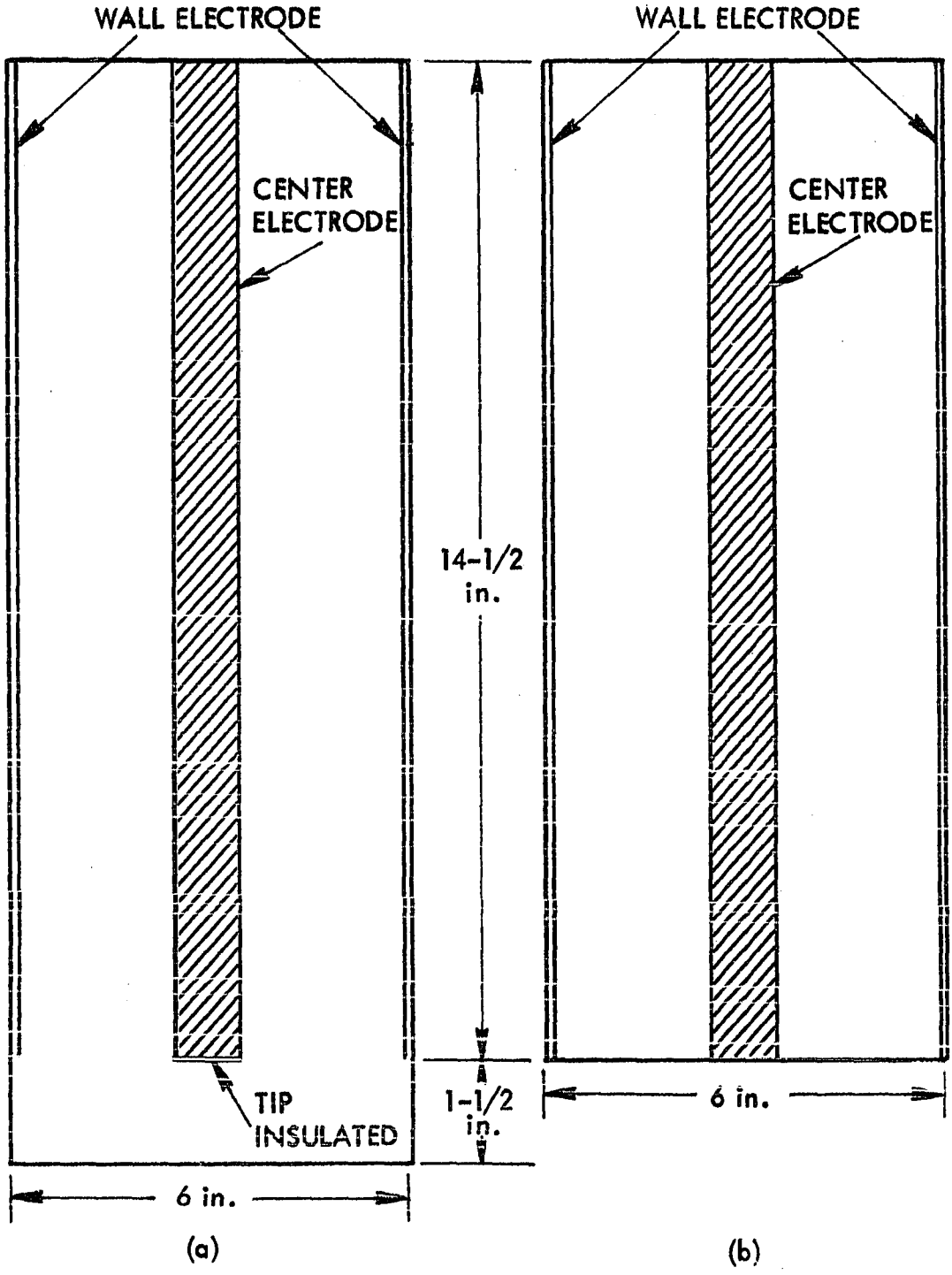
WALL ELECTRODE
CENTER ELECTRODE
TIP INSULATED
14-1/2 in.
1-1/2 in.
6 in.
(a)
WALL ELECTRODE
CENTER ELECTRODE
6 in.
(b)

r = radial position of the probe measured from the center-line of the test column

a = radius of the center electrode

b = radius of the wall electrode

By cross-plotting the data from Figures 11-17, the voltage profile inside the bed were obtained for any given gas flowrate. Shown in Figure 19 is a typical one chosen at a gas flowrate of 1.49 SCFM. The fairly straight line in the plot is what would be expected from equation (21). Extrapolating this straight line to the surface of the wall and center electrodes gives two intercepts which correspond respectively to the values of V_a and V_b. Also shown in the figure is the total applied voltage, V_o. The difference between V_o and V_a is the total voltage drop due to the contact resistance at the center electrode. The value of V_b was always much smaller than the value of $V_o - V_a$. This fact indicated that the contact resistance at the wall electrode was always much smaller than the one at the center electrode. Since the resistance is inversely proportional to the cross-sectional area, this fact can be attributed to the comparably large surface area of the wall electrode.

For calculating the contact resistance and bed resistivity, the following equations were used:

$$R_b = (V_a - V_b)/I = \rho_b \ln (b/a)/2\pi L \qquad (22)$$

$$R_{ce} = (V_o - V_a)/I \qquad (23)$$

$$R_{cw} = V_b/I \qquad (24)$$

Figure 19. Potential in fluidized bed as a function of radial position for -65+80 mesh calcined coke at a gas flowrate of 1.49 SCFM

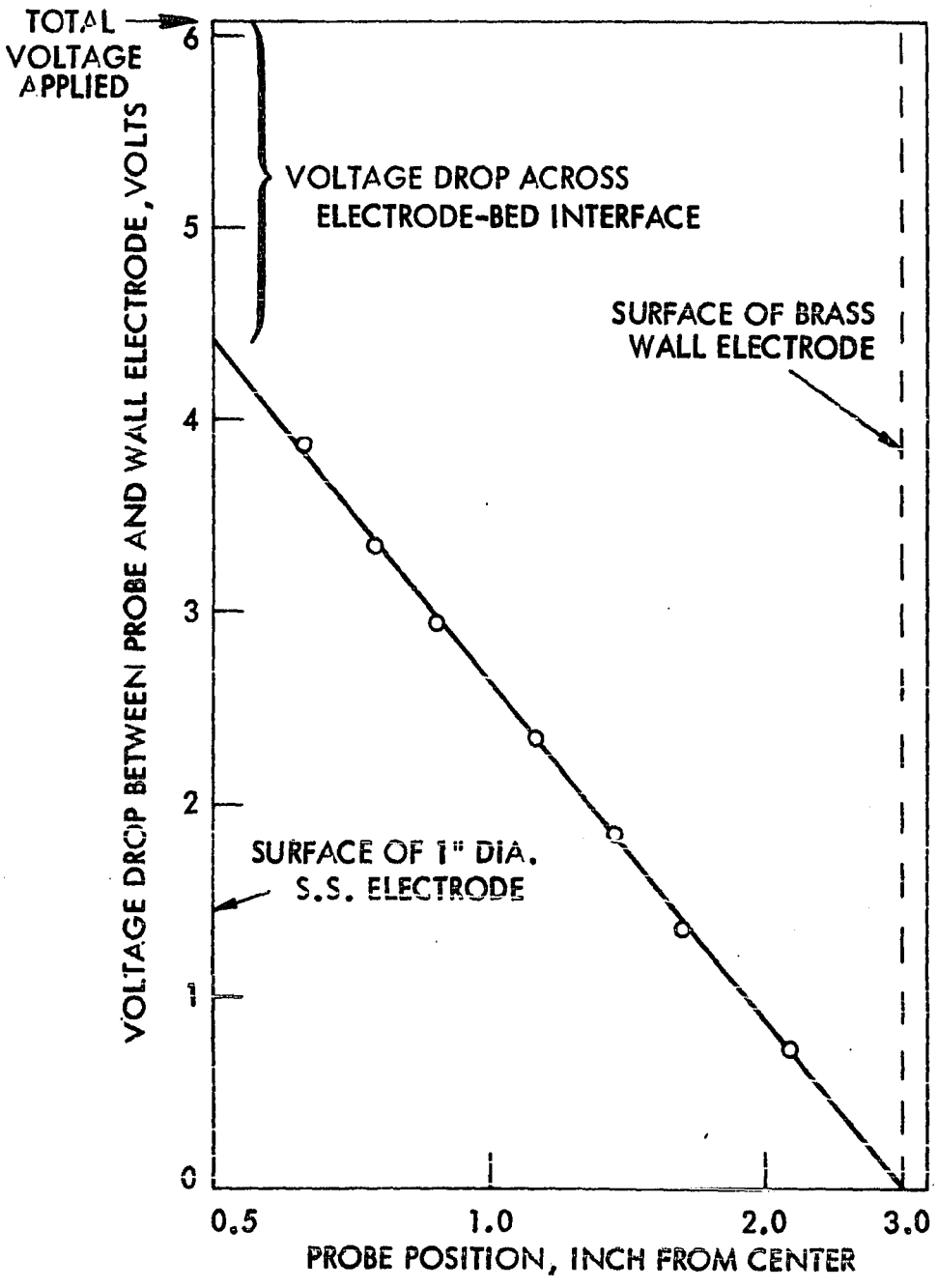
TOTAL VOLTAGE APPLIED
VOLTAGE DROP ACROSS ELECTRODE-BED INTERFACE
SURFACE OF BRASS WALL ELECTRODE
SURFACE OF 1" DIA. S.S. ELECTRODE
VOLTAGE DROP BETWEEN PROBE AND WALL ELECTRODE, VOLTS
0
1
2
3
4
5
6
0.5
1.0
2.0
3.0
PROBE POSITION, INCH FROM CENTER

where L is the length of the electrode. Equation (22) is the Ohm's Law regarding the resistance of a concentric system. The resulting relationships between gas velocity and bed resistivity and contact resistance at the center electrode are shown in Figures 8 and 20, respectively. The contact resistance at the wall electrode is not given here because it was too small to be detected.

Figure 20. Effect of gas flowrate on contact resistance for 1-inch diameter center electrode in the -65+80 mesh calcined coke bed at current of 0.58 amperes (Runs 2, 3, 4 and 5)

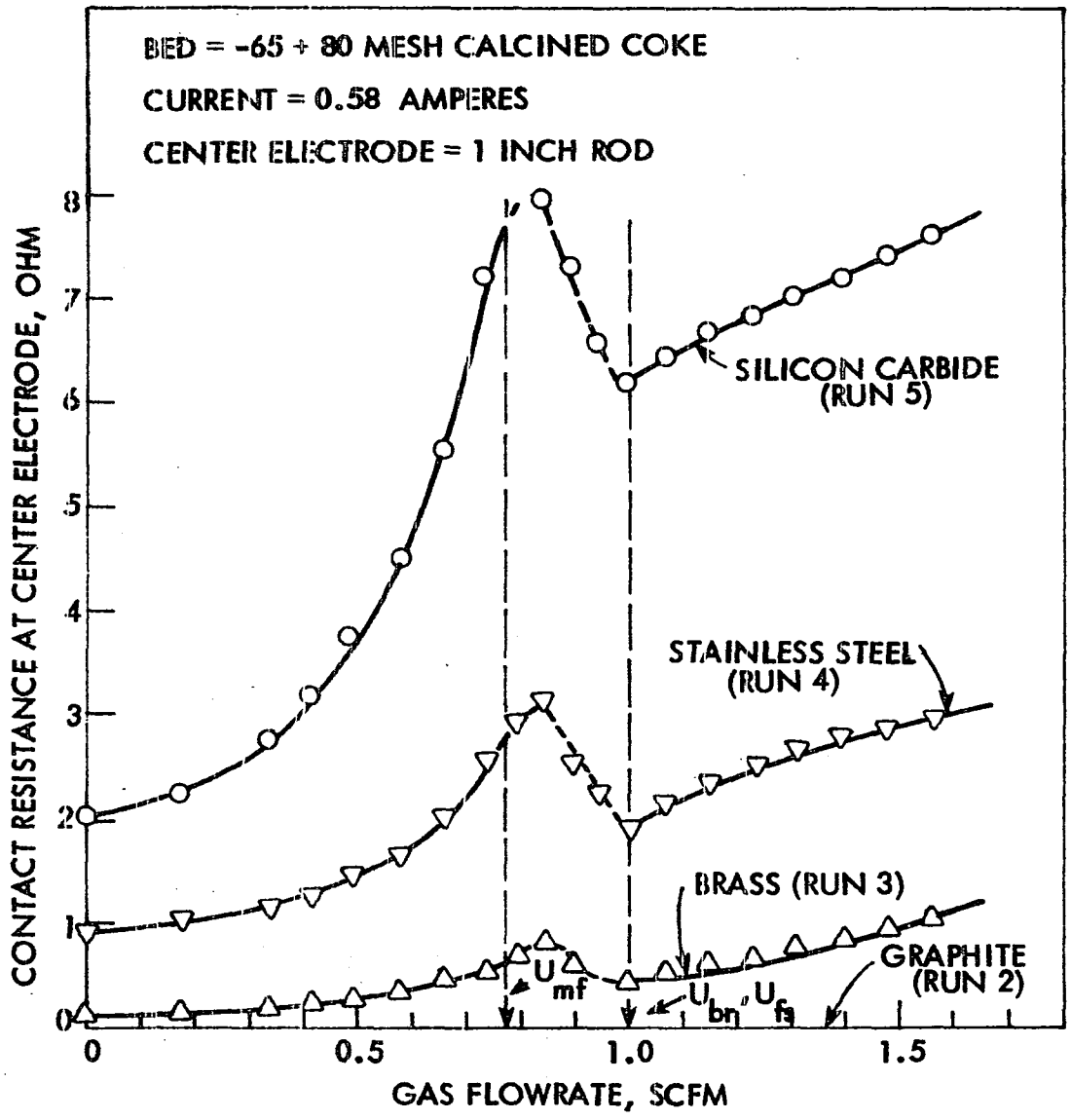
BED = -65 + 80 MESH CALCINED COKE
CURRENT = 0.58 AMPERES
CENTER ELECTRODE = 1 INCH ROD
CONTACT RESISTANCE AT CENTER ELECTRODE, OHM
GAS FLOWRATE, SCFM
SILICON CARBIDE (RUN 5)
STAINLESS STEEL (RUN 4)
BRASS (RUN 3)
GRAPHITE (RUN 2)
U_{mf}
U_{bn}, U_{fs}
0
1
2
3
4
5
6
7
8
0
0.5
1.0
1.5

RESULTS AND DISCUSSION

Bed and contact resistances were measured in the previously described apparatus as a function of gas flowrate using various combinations of bed material, type and diameter of center electrode and current density. These combinations marked the differences among the 15 runs shown in Table 3. The experimental conditions of the runs shown in the table were so chosen that the effect of a particular factor could be observed by comparing certain runs; for example, in Runs 12 to 15, only the magnitude of the current was changed from one run to another. Totally, three bed materials (-65+80 mesh calcined coke, -65+80 mesh graphite and -35+200 mesh calcined coke), four center electrode materials (graphite, brass, stainless steel and silicon carbide), three center electrode diameters (0.5, 1.0 and 1.5 inches) and four currents (0.29, 0.58, 0.87 and 1.16 amperes) were tried. Results of Run 4 have already been presented in the last section without detailed discussion. The results from the rest of the runs will be presented here, along with the result obtained by fitting the data collected in the same experiments to the semi-empirical correlation for bed resistivity proposed earlier in this report.

The geometry of the fluidization column in Runs 2 to 5 was identical and hence a common fluidization pattern was expected. The fact that the same pressure drop and bed height were observed at a given gas flowrate for all these runs indicated that this was true. This also was true for Runs 7 to 10 and Runs 12 to 15.

Table 3. Experimental conditions used in measuring contact resistance and bed resistivity

Run	Bed material	Center electrode	Current, A	U_{mf}, cm/sec
1	Calcined coke (-65+80 mesh)	0.5-inch diam. brass rod	0.58	2.08
2	Calcined coke (-65+80 mesh)	1.0-inch diam. graphite rod	0.58	1.98
3	Calcined coke (-65+80 mesh)	1.0-inch diam. brass rod	0.58	1.98
4	Calcined coke (-65+80 mesh)	1.0-inch diam. stainless steel	0.58	1.98
5	Calcined coke (-65+80 mesh)	1.0-inch diam. silicon carbide	0.58	1.98
6	Graphite (-65+80 mesh)	0.5-inch diam. brass rod	0.58	2.94
7	Graphite (-65+80 mesh)	1.0-inch diam. graphite rod	0.58	2.87
8	Graphite (-65+80 mesh)	1.0-inch diam. brass rod	0.58	2.87
9	Graphite (-65+80 mesh)	1.0-inch diam. stainless steel	0.58	2.87
10	Graphite (-65+80 mesh)	1.0-inch diam. silicon carbide	0.58	2.87
11	Graphite (-65+80 mesh)	1.5-inch diam. brass rod	0.58	2.79
12	Calcined coke (-35+200 mesh)	1.0-inch diam. stainless steel	0.29	1.95
13	Calcined coke (-35+200 mesh)	1.0-inch diam. stainless steel	0.58	1.95

Table 3. (Continued)

Run	Bed material	Center electrode	Current, A	U_{mf}, cm/sec
14	Calcined coke (-35+200 mesh)	1.0-inch diam. stainless steel	0.87	1.95
15	Calcined coke (-35+200 mesh)	1.0-inch diam. stainless steel	1.16	1.95

Also listed in Table 3 are the minimum fluidization velocities, U_{mf}, conventionally determined from the corresponding pressure drop versus gas flowrate plots (Figures 8, 21, 22, 23, 24 and 25) (5); in these plots the minimum fluidization velocity is the gas flowrate at which the two straight lines in the low and high gas flowrate regions intersect with each other. As can be seen from Table 3, the only experimental condition which varied between Runs 1 and 3 or among Runs 6, 8 and 11 was the center electrode diameter. The results from both sets of runs indicated that the U_{mf} decreased if a larger center electrode was used, although the changes were small. This trend might be due to different extents of bed disturbance caused by immersion of the center electrode in the bed.

The effect of particle size distribution on U_{mf} can be seen from a comparison of Run 3 and Runs 12 to 15. The minimum fluidization velocities for these runs were about the same even though the latter four runs had a wider particle size distribution. The harmonic average particle size, $\bar{d}_p$, is usually suggested for characterizing the bed particle size in the correlation of U_{mf} (29). $\bar{d}_p$ was calculated as follows:

Figure 21. Effect of gas flowrate on bed resistivity and pressure drop for 0.5-inch diameter center electrode in the -65+80 mesh calcined coke bed at current of 0.58 amperes (Run 1)

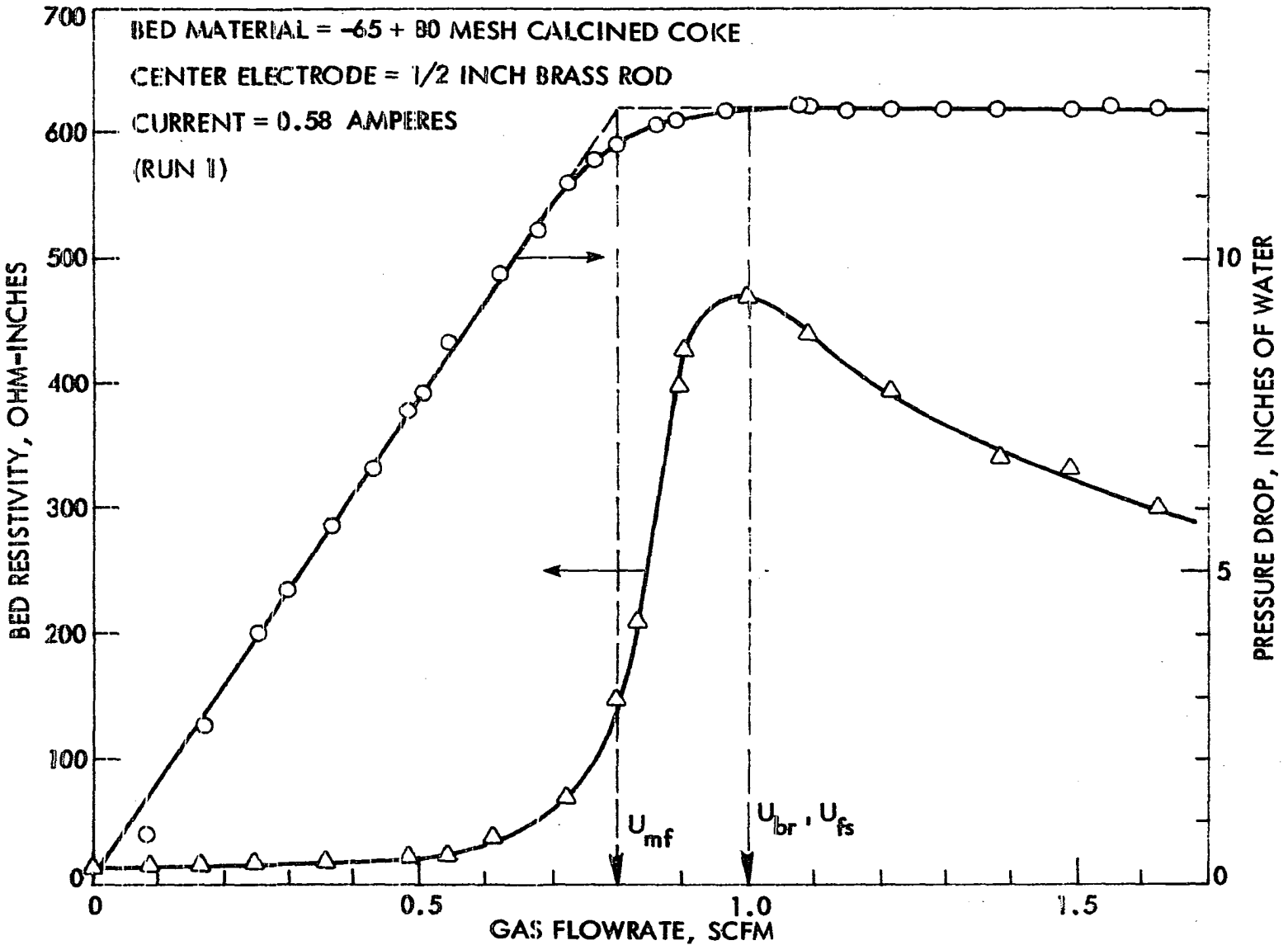
BED MATERIAL = -65 + 80 MESH CALCINED COKE
CENTER ELECTRODE = 1/2 INCH BRASS ROD
CURRENT = 0.58 AMPERES
(RUN 1)
BED RESISTIVITY, OHM-INCHES
PRESSURE DROP, INCHES OF WATER
GAS FLOWRATE, SCFM
700
600
500
400
300
200
100
0
10
5
0
0.5
1.0
1.5
U_{mf}
U_{br} , U_{fs}

Figure 22. Effect of gas flowrate on bed resistivity and pressure drop for 0.5-inch diameter center electrode in the -65+80 mesh graphite bed at current of 0.58 amperes (Run 6)

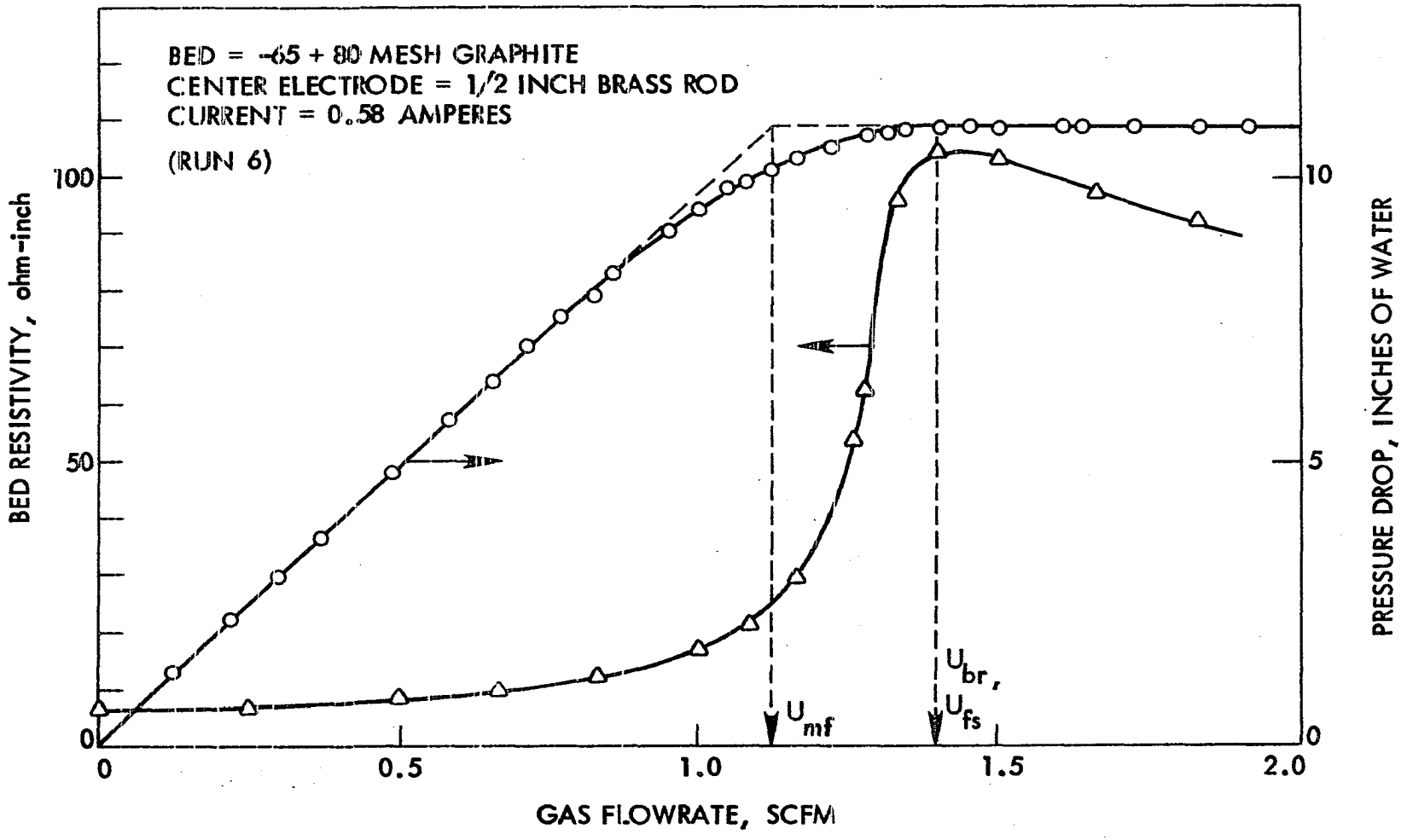
BED = -65 + 80 MESH GRAPHITE
CENTER ELECTRODE = 1/2 INCH BRASS ROD
CURRENT = 0.58 AMPERES
(RUN 6)
BED RESISTIVITY, ohm-inch
PRESSURE DROP, INCHES OF WATER
GAS FLOWRATE, SCFM
100
50
0
10
5
0
0.5
1.0
1.5
2.0
U_{mf}
U_{br},
U_{fs}

Figure 23. Effect of gas flowrate on bed resistivity and pressure drop for 1.0-inch diameter center electrode in the -65+80 mesh graphite bed at current of 0.58 amperes (Runs 7, 8, 9 and 10)

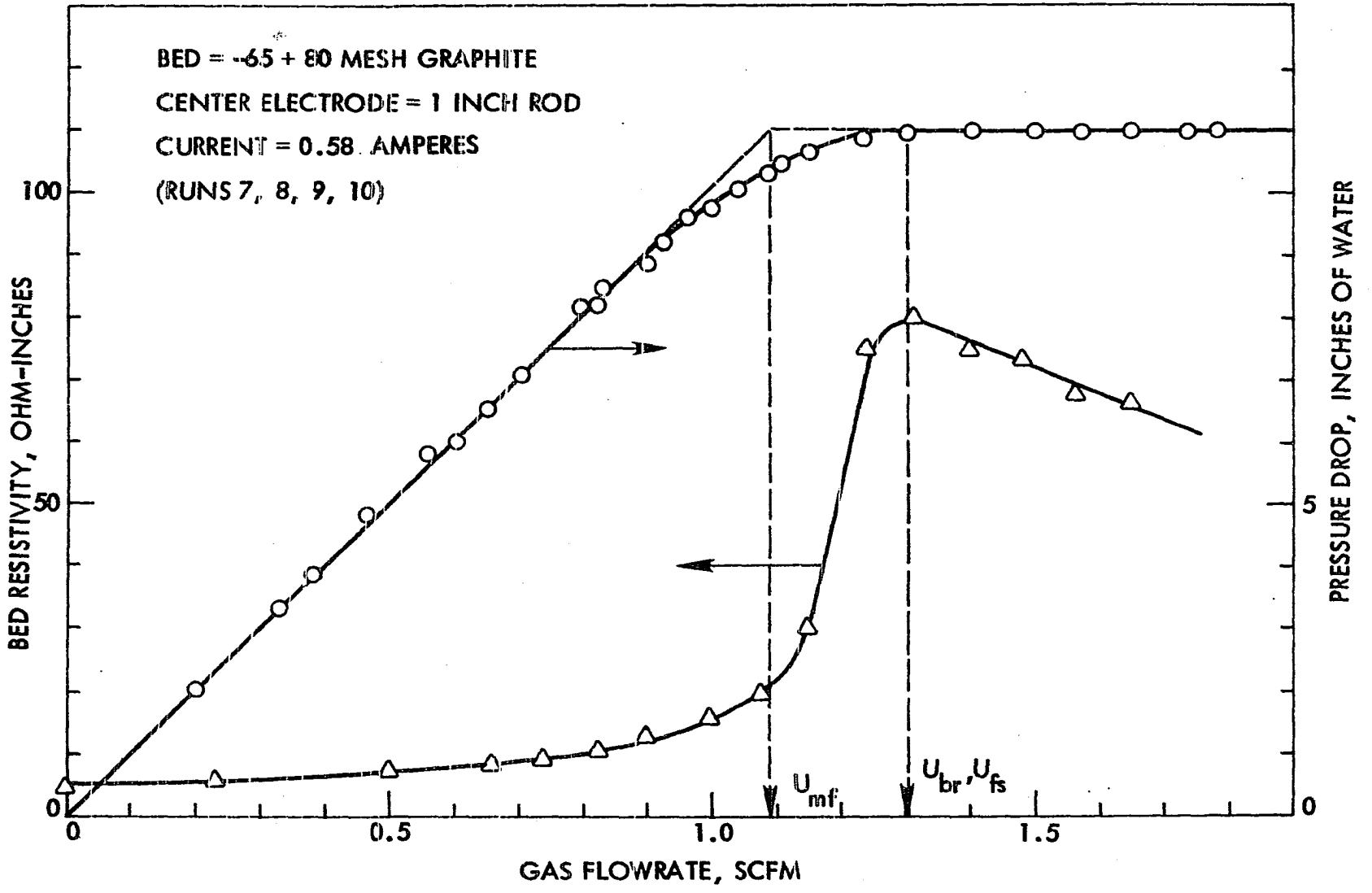
BED = -65 + 80 MESH GRAPHITE
CENTER ELECTRODE = 1 INCH ROD
CURRENT = 0.58 AMPERES
(RUNS 7, 8, 9, 10)
BED RESISTIVITY, OHM-INCHES
100
50
0
PRESSURE DROP, INCHES OF WATER
5
0
0
0.5
1.0
1.5
GAS FLOWRATE, SCFM
U_{mf}
U_{br}, U_{fs}

Figure 24. Effect of gas flowrate on bed resistivity and pressure drop for 1.5-inch diameter center electrode in the -65+80 mesh graphite bed at current of 0.58 amperes (Run 11)

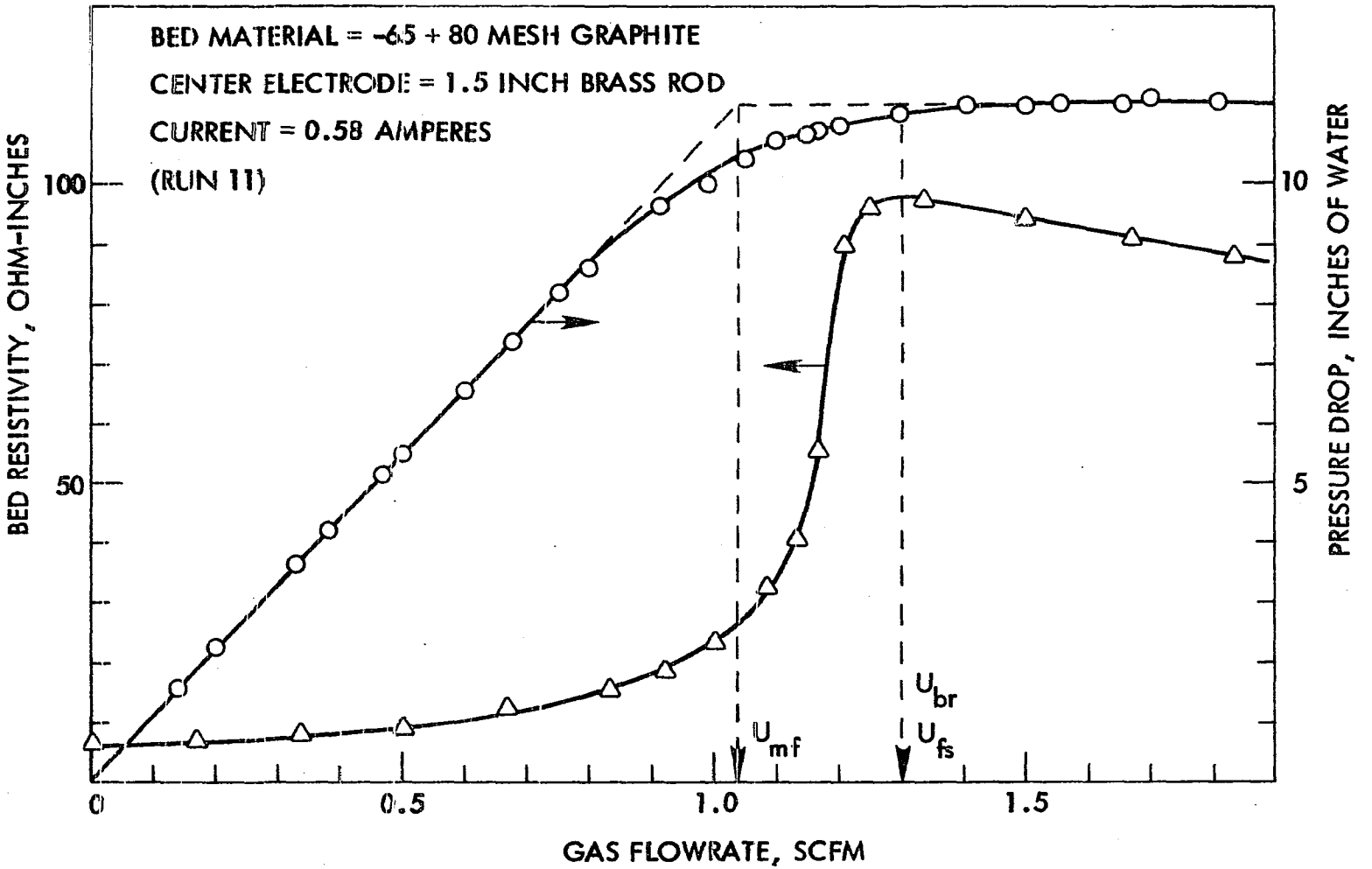
BED MATERIAL = -65 + 80 MESH GRAPHITE
CENTER ELECTRODE = 1.5 INCH BRASS ROD
CURRENT = 0.58 AMPERES
(RUN 11)
BED RESISTIVITY, OHM-INCHES
100
50
0
0.5
1.0
1.5
GAS FLOWRATE, SCFM
U_{mf}
U_{br}
U_{fs}
10
5
PRESSURE DROP, INCHES OF WATER

Figure 25. Effect of gas flowrate on bed resistivity and pressure drop for 1.0-inch diameter center electrode in the -35+200 mesh calcined coke bed at four different currents (Runs 12, 13, 14 and 15)

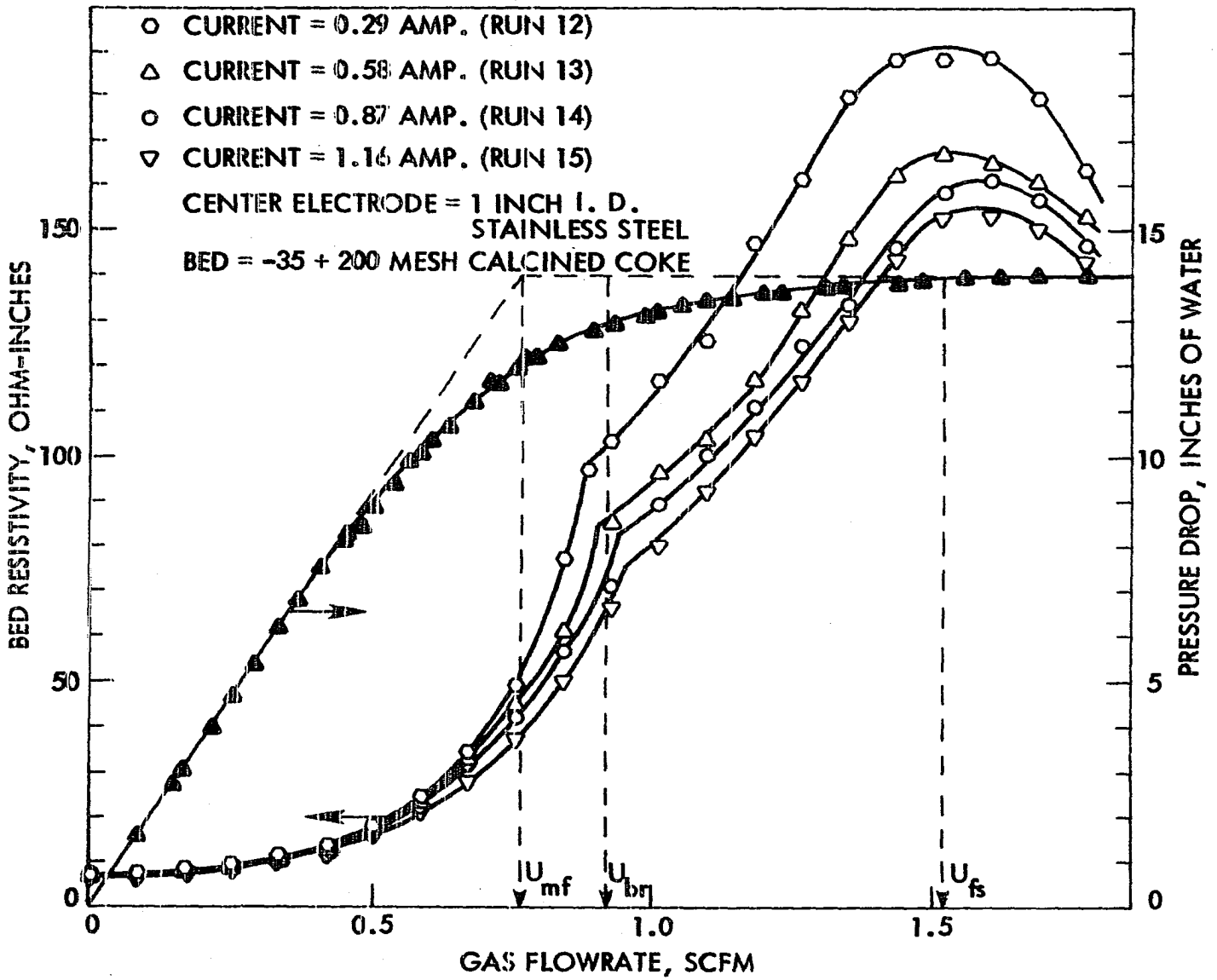
CURRENT = 0.29 AMP. (RUN 12)
CURRENT = 0.58 AMP. (RUN 13)
CURRENT = 0.87 AMP. (RUN 14)
CURRENT = 1.16 AMP. (RUN 15)
CENTER ELECTRODE = 1 INCH I. D. STAINLESS STEEL
BED = -35 + 200 MESH CALCINED COKE
BED RESISTIVITY, OHM-INCHES
PRESSURE DROP, INCHES OF WATER
GAS FLOWRATE, SCFM
0
50
100
150
0
5
10
15
0
0.5
1.0
1.5
U_{mf}
U_{br}
U_{fs}

$$\bar{d}_p = \frac{1}{\int_0^{d_p,max} \frac{D(d_p)}{d_p}\, d(d_p)} \qquad (18)$$

where $D(d_p)$ represents the particle size distribution function of the bed material. The harmonic average particle size is different from the simple mean particle size because it involves the use of a weighting function, $1/d_p$, during the averaging procedure. A $\bar{d}_p$ of 170 microns was found for the -65+80 mesh calcined coke bed, while for the -35+200 mesh calcined coke bed it was 165 microns. Since the two beds had approximately the same $\bar{d}_p$, they would be expected to have the same U_{mf} as is indicated in Table 3.

In addition to U_{mf}, two more velocities which will be referred to in the later discussion of gas flowrate effects on bed resistivity and contact resistance are also noted in the above-mentioned pressure drop diagrams. The velocity labeled U_{br} is the gas velocity at which gas bubbles are first observed passing through the bed, while the one marked U_{fs} represents the fluidization stage where the bed weight is fully supported by the gas stream and the pressure drop through the bed approaches an equilibrium value.

It is generally recognized that during the course of fluidization, the small bed particles are the first to fluidize (5). This happens at the minimum fluidization velocity. The largest particles do not fluidize until the velocity reaches U_{fs}. In line with this, it was observed in this investigation that U_{fs} was 1.2 times U_{mf} for the beds with narrow particle size distribution (-65+80 mesh material), while

U_{fs} was twice U_{mf} for the material with a wide particle size distribution (-35+200 mesh calcined coke).

Bed Resistivity

The bed resistivities for all the runs cited in Table 3 are summarized in Figures 8, 21, 22, 23, 24 and 25 where they are shown as a function of gas flowrate. The bed resistivities in Runs 2 to 5 were identical despite the use of different center electrode materials (Figure 8). This was expected since the same fluidization conditions prevailed in the test column in all these runs and the same amount of current was used. This was also true for Runs 7 to 10 (Figure 23).

Effect of gas flowrate

For the beds of -65+80 mesh calcined coke and -65+80 mesh graphite, the bed resistivity did not change significantly as the gas flowrate was increased until the minimum fluidization velocity was reached (Figures 8, 21, 22, 23 and 24). As the gas flowrate was increased further, the bed resistivity increased rapidly to a peak value of U_{fs} and then decreased. For these two beds, the gas bubbles also started to rise at U_{fs}. The -35+200 mesh calcined coke bed gave results similar to those noted for the other two beds, namely, a sharp increase in bed resistivity at U_{mf} and a peak value at U_{fs}. However, with this material U_{br} was different from U_{fs} and a break point in the bed resistivity curve was found at U_{br} (Figure 25).

Except for the break points that appeared in the last four runs, the variation of bed resistivity with gas flowrate obtained in this

investigation was similar to that observed by a number of other research workers (13, 14, 23, 45). The beds investigated by Graham and Harvey (13, 14) and Smith (45) all had a narrow particle size distribution and the peak bed resistivity was reported to occur at a gas velocity slightly higher than the minimum fluidization velocity. Jones and Wheelock (23) used beds with both narrow and wide particle size distributions, and their results with the former beds agreed closely to what was reported by Graham and Harvey and Smith. The wide particle size distribution beds gave a peak bed resistivity at a velocity two to three times the minimum fluidization velocity. In the experiments reported here, a similar trend was observed since the peak bed resistivity occurred at 1.2 U_{mf} for the runs with -65+80 mesh calcined coke and graphite beds (narrow particle size distribution), and at 2 U_{mf} for the runs with -35+200 mesh calcined coke beds (wide particle size distribution).

Effect of current

The effect of current can be seen from the four curves in Figure 25. The magnitudes of the currents used had a ratio of 1:2:3:4. The result revealed that, in the gas flowrate range being investigated, the bed resistivity always decreased as current was increased. This effect was thought to be an indication that some arcing was present in the bed since arcing is more likely to occur at higher current densities (19, 31, 51, 53), which would give a smaller bed resistivity by providing an additional route for the current flow. The same effect of current on bed resistivity has been observed and reported by many

research workers (9, 42, 45). A similar effect of current on inter-electrode resistance has also been reported by Goldschmidt and LeGoff (11) and Zheltov, et al. (53).

Effect of bed material

Bed resistivities obtained with the -65+80 mesh calcined coke bed (Figures 8 and 21) were found to be higher than those with the -65+80 mesh graphite bed (Figures 22, 23 and 24). This is probably attributable to the higher electrical conductivity of the graphite particles.

The runs presented in Figures 8 and 25 all used a calcined coke bed, but the ones in the latter diagram were made with a bed having a much wider particle size distribution and gave a much smaller bed resistivity. It is generally reported in the literature that the voidage is smaller in a bed with a wide variation of particle sizes since the fine material can fit into the voids between the large particles (5, 29, 32, 52). The lower bed resistivity found in the runs shown in Figure 24 could be related, then, to the lower voidages of these beds. This would facilitate current flow by giving more contacts between particles if conducting chains are the main mechanism of flow, or by shortening the space between particles if arcing is important.

Jones and Wheelock (23) also investigated the effect of particle size distribution. They compared the peak heights in the bed resistivity-gas flowrate curve between the narrow and wide particle

size distribution beds and found the latter bed provided a much higher peak. A similar result was not observed in this investigation.

The semi-empirical correlation for the bed resistivity

After having experimentally determined the bed resistivity, pressure drop and bed height as a function of fluidization velocity, equation (13) was used to calculate f_d which was then plotted as a function of the relative fluidization velocity. The final result is shown in Figure 26. It indicates that f_d depended somewhat on the type of bed material used (graphite or calcined coke), but for both materials it gradually diminished from one to zero as the relative fluidization velocity went from zero to 1.22. This latter velocity was the point where the gas bubbles first appeared during the experiments and where the basic structure of the settled bed was believed to be totally destroyed.

The original derivation of the semi-empirical correlation for the bed resistivity assumed that the conducting chains were the only mechanism for current flow through the bed. However, since the magnitude of the current flow was observed to affect the bed resistivity, it seemed that the bed resistivity data were collected when arcing also was contributing to current flow. With a bed that had a tendency to arc, regions inside the bed which originally were considered inaccessible to current flow could become electrically conducting through arcing. As $(1 - f_d)$ represents the volume fraction of the nonconducting regions in the bed, f_d would then be affected by some of the physical properties usually used to characterize the arcing potential of the bed material.

Figure 26. Experimentally determined relation between f_d and relative fluidization velocity

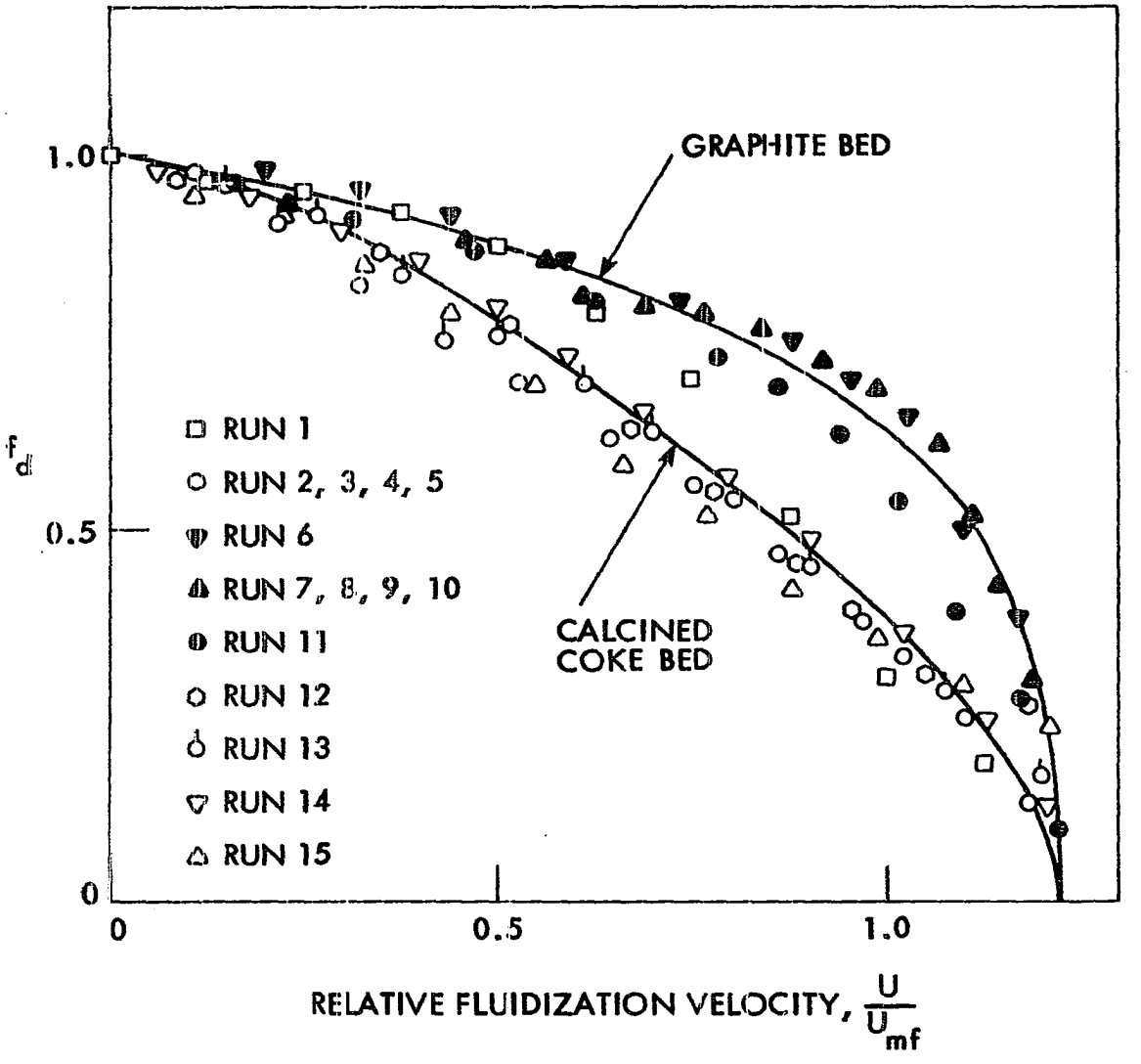
GRAPHITE BED
CALCINED COKE BED
RUN 1
RUN 2, 3, 4, 5
RUN 6
RUN 7, 8, 9, 10
RUN 11
RUN 12
RUN 13
RUN 14
RUN 15
f_d
1.0
0.5
0
0
0.5
1.0
RELATIVE FLUIDIZATION VELOCITY, $\frac{U}{U_{mf}}$

This may explain why the experimentally determined f_d depended not only on the relative fluidization velocity, but also on the type of material being fluidized.

In the case of the data shown in Figure 26, f_d is higher for the graphite beds. This may indicate that more arcing was taking place in these beds.

Contact Resistance

The contact resistances at the center electrode for all the runs cited in Table 3 are summarized in Figures 20, 27, 28, 29 and 30 where they are shown as a function of gas flowrate. In Figures 20 and 27, Runs 2, 7 and 11 are shown as having zero contact resistance since the measured contact resistances were less than 1% of the corresponding total resistances and were comparable to the magnitude of the associated experimental errors. This was also true for the contact resistances measured at the wall electrode in all the runs; therefore, they are not presented here. Reasons for such a small contact resistance will be discussed later.

Effect of gas flowrate

Generally speaking, the contact resistances for all the runs tended to increase as the gas flowrate was increased (Figures 20, 27, 28, 29 and 30). However, in the first eleven runs (Figures 20, 27, 28 and 29) the contact resistance did not always continuously increase with gas velocity in the region between U_{mf} and U_{fs} and the behavior of the resistance tended to be somewhat erratic in this velocity region. The

Figure 27. Effect of gas flowrate on contact resistance for the 0.5-inch diameter brass center electrode in the -65+80 mesh calcined coke bed at current of 0.58 amperes (Run 1)

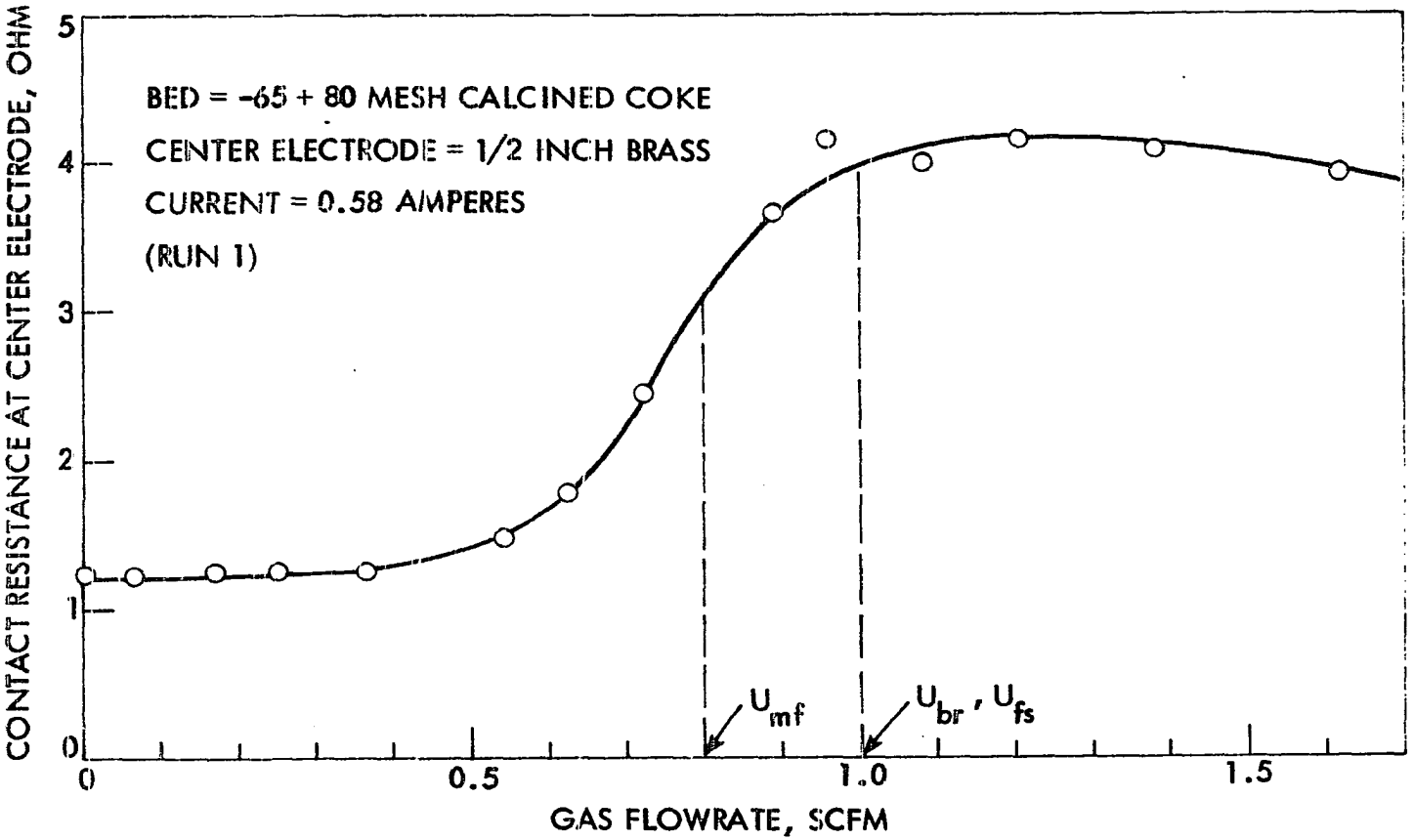
BED = -65 + 80 MESH CALCINED COKE
CENTER ELECTRODE = 1/2 INCH BRASS
CURRENT = 0.58 AMPERES
(RUN 1)
CONTACT RESISTANCE AT CENTER ELECTRODE, OHM
GAS FLOWRATE, SCFM
U_{mf}
U_{br} , U_{fs}
0
0.5
1.0
1.5
1
2
3
4
5

Figure 28. Effect of gas flowrate on contact resistance for the 0.5-inch diameter center electrode in the -65+80 mesh graphite bed at current of 0.58 amperes (Run 6)

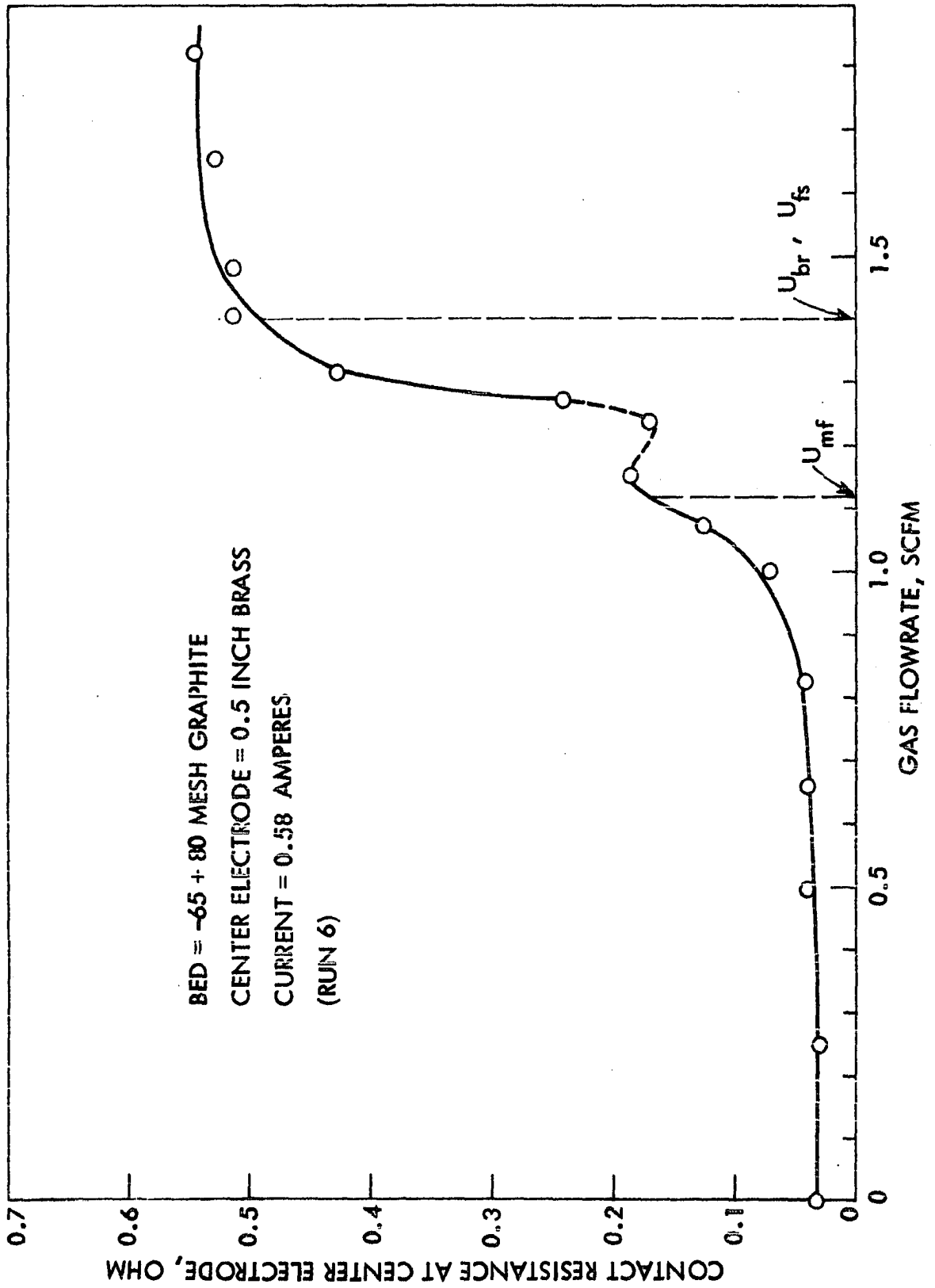
BED = -65 + 80 MESH GRAPHITE
CENTER ELECTRODE = 0.5 INCH BRASS
CURRENT = 0.58 AMPERES
(RUN 6)
U_{br} , U_{fs}
U_{mf}
CONTACT RESISTANCE AT CENTER ELECTRODE, OHM
GAS FLOWRATE, SCFM
0.7
0.6
0.5
0.4
0.3
0.2
0.1
0
0.5
1.0
1.5

Figure 29. Effect of gas flowrate on contact resistance for the 1-inch diameter center electrodes in the -65+80 mesh graphite bed at current of 0.58 amperes (Runs 7, 8, 9 and 10)

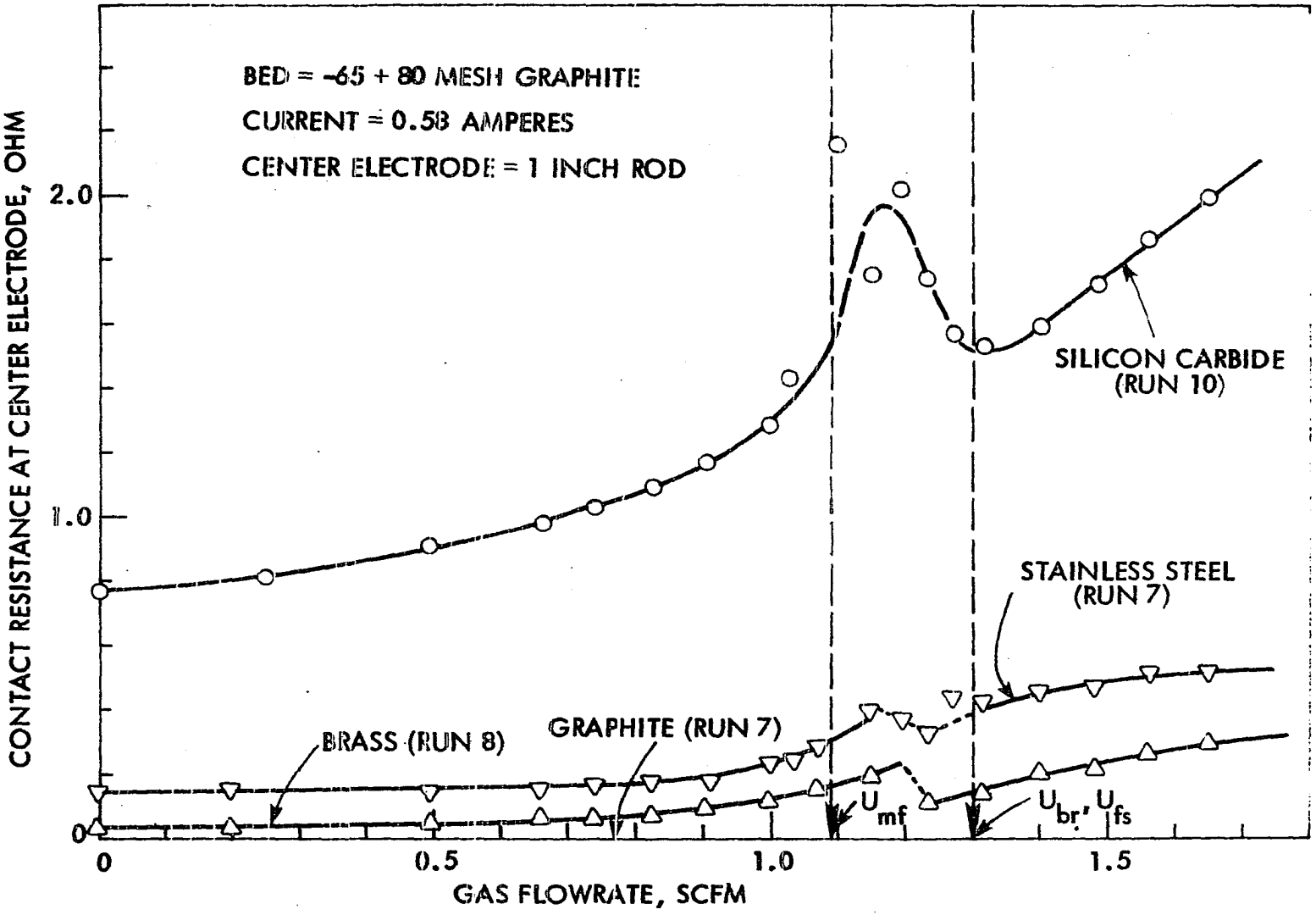
BED = -65 + 80 MESH GRAPHITE
CURRENT = 0.58 AMPERES
CENTER ELECTRODE = 1 INCH ROD
CONTACT RESISTANCE AT CENTER ELECTRODE, OHM
2.0
1.0
0
SILICON CARBIDE (RUN 10)
STAINLESS STEEL (RUN 7)
BRASS (RUN 8)
GRAPHITE (RUN 7)
U_{mf}
U_{br}, U_{fs}
0
0.5
1.0
1.5
GAS FLOWRATE, SCFM

Figure 30. Effect of gas flowrate on contact resistance for the 1-inch diameter center electrode in the -35+200 mesh calcined coke bed at four different currents (Runs 12, 13, 14 and 15)

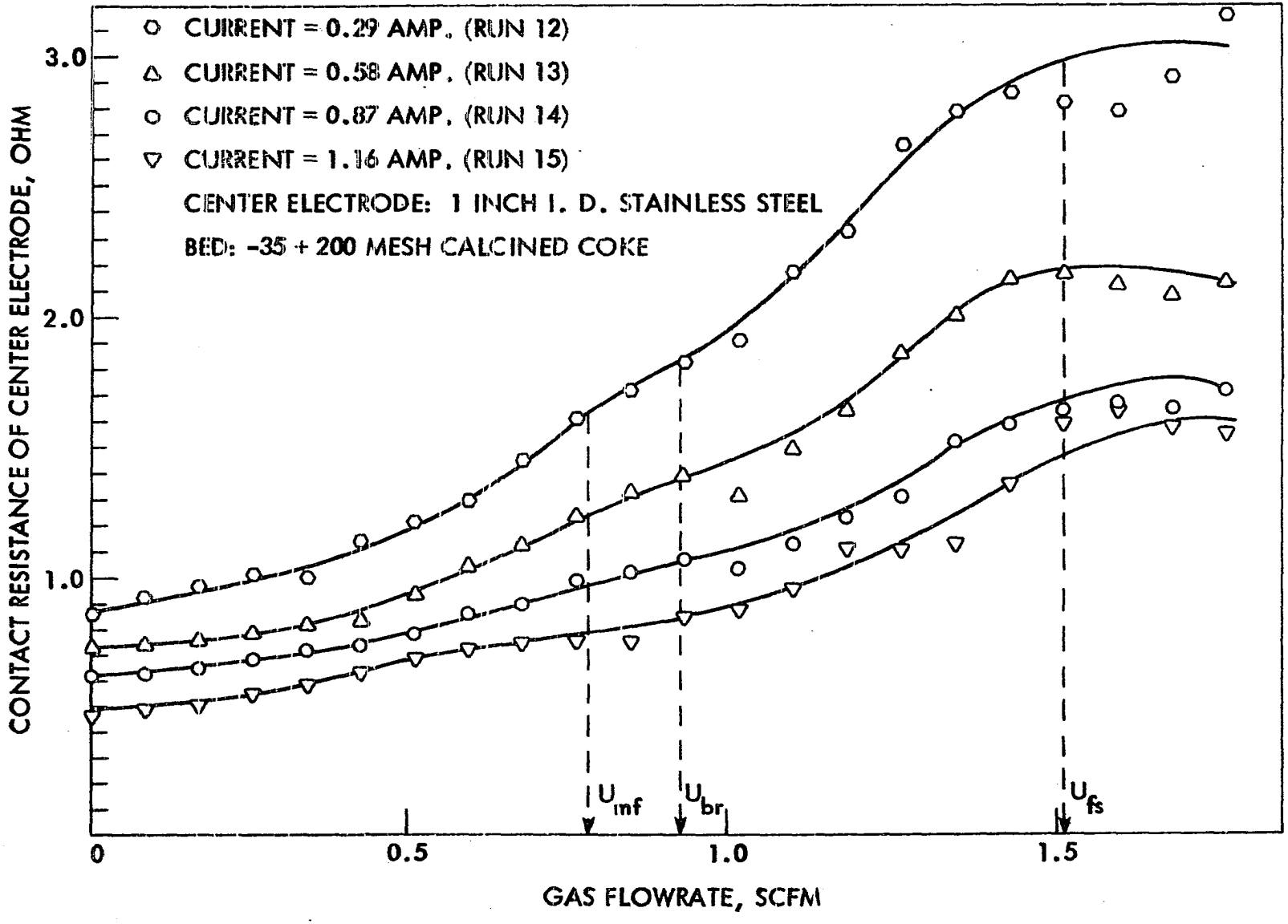
CURRENT = 0.29 AMP. (RUN 12)
CURRENT = 0.58 AMP. (RUN 13)
CURRENT = 0.87 AMP. (RUN 14)
CURRENT = 1.16 AMP. (RUN 15)
CENTER ELECTRODE: 1 INCH I. D. STAINLESS STEEL
BED: -35 + 200 MESH CALCINED COKE
CONTACT RESISTANCE OF CENTER ELECTRODE, OHM
3.0
2.0
1.0
0
0.5
1.0
1.5
GAS FLOWRATE, SCFM
U_{mf}
U_{br}
U_{fs}

data points in this region have some degree of uncertainty caused by the unreliable measurement of the voltage drop from which these contact resistances were derived (a typical situation is shown in Figure 10). These unreliable measurements were a natural consequence of the drastic change in the electrical properties of the bed as indicated by the sharp rise of both curves in Figure 10 in the gas flowrate region between U_{mf} and U_{fs}.

The results from Runs 1 and 6 differed from those of Runs 2 to 5 and 7 to 10 since the contact resistance in the first two runs increased much more when the gas flowrate went from a low to a high value (compare Figures 27 and 28 with 20 and 29). Since the major difference between the experimental conditions for these two sets of runs was the diameter of the center electrode, the electrode size is thought to affect the fluidization and therefore the change of the contact resistance with the gas flowrate.

Effect of bed material

For a given center electrode, the contact resistance of the -65+80 mesh graphite bed was always much less than that of the -65+80 mesh calcined coke bed (comparing Run 1 with Run 6, 2 with 7, 3 with 8, 4 with 9, and 5 with 10). Since the bed resistivity of graphite was also much less than that of calcined coke, a relationship seemed to exist between the contact resistance and the bed resistivity. In Figure 31, the ratio of the contact resistance to total resistance is plotted against the relative fluidization velocity for the pairs of runs mentioned above. The ratio was indeed about the same for the runs

Figure 31. Ratios of contact resistance to total resistance versus relative fluidization velocity for Runs 1, 3, 4, 5, 6, 8, 9 and 10

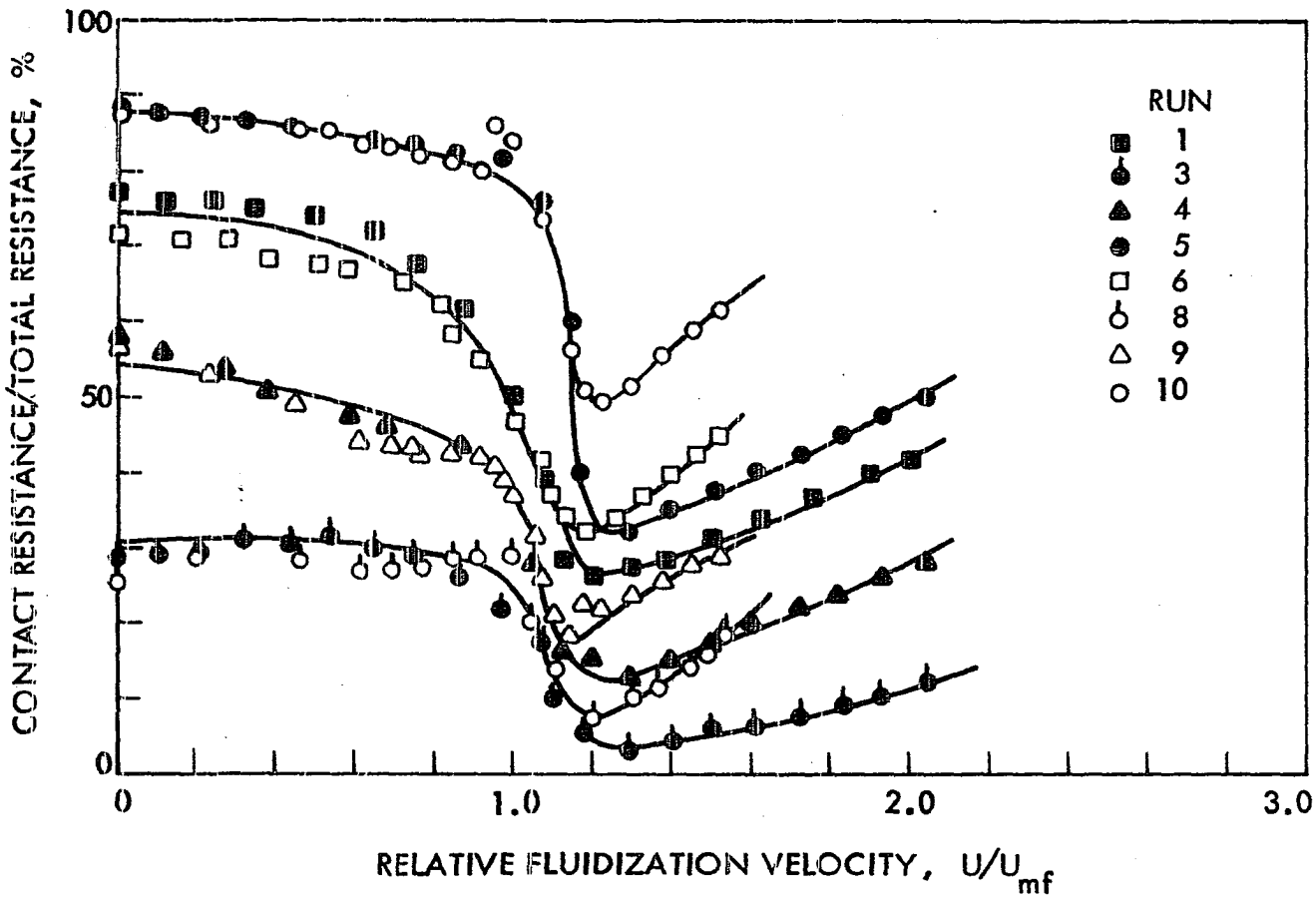
100
50
0
0
1.0
2.0
3.0
CONTACT RESISTANCE/TOTAL RESISTANCE, %
RELATIVE FLUIDIZATION VELOCITY, U/U$_{mf}$
RUN
1
3
4
5
6
8
9
10

having center electrodes of the same material and diameter for gas velocities up to U_{br}. Since the bed height and the wall and center electrode diameters are the same for the runs being compared, the identity as observed for the ratio of contact resistance to total resistance also implied that the ratios of contact resistance to the bed resistivity are the same through the following equation which is derived from equation (22)

$$\frac{R_c}{\rho_b} = \frac{\ln(\frac{b}{a})}{2\pi L} \frac{(\frac{R_c}{R_t})}{1 - (\frac{R_c}{R_t})} \qquad (22)$$

Therefore, it appears that the contact resistance is linearly proportional to the bed resistivity for gas velocities less than U_{br}. This simple relation does not hold beyond this velocity, probably due to the formation of gas bubbles in the bed.

Effect of electrode material

Four center electrode materials, silicon carbide, stainless steel, brass and graphite, were tested in both the -65+80 mesh calcined coke bed and the -65+80 mesh graphite bed. The diameter of all four electrodes was the same. Results (Figures 21 and 27) with these beds consistently showed that the silicon carbide rod always had the largest contact resistance, followed in order of decreasing contact resistance by the stainless steel, brass and graphite rods. A similar result with graphite, brass and stainless steel center electrodes also was reported by Yuan (51). The observed effect of electrode material on contact resistance is possibly explained by the difference

in hardness among the electrodes since Holm (16) has pointed out that the contact resistance is larger for a harder material. Silicon carbide was the hardest material among those tested as center electrodes, followed in order by stainless steel, brass and graphite.

Effect of electrode diameter

In this investigation, brass rods were used as electrodes to test the effect of electrode diameter on contact resistance. Two sizes of electrodes (0.5- and 1.0-inch O.D. rods) were tried in the -65+80 mesh calcined coke bed, while three electrodes, each with a different diameter (0.5-, 1.0- and 1.5-inch O.D. rods), were used in the -65+80 mesh graphite bed. Results from both beds (Figures 20, 27, 28 and 29) indicated that the contact resistance decreased as the electrode diameter, and hence surface area, was increased. Additional evidence for this conclusion was the small contact resistance observed at the wall electrode. Since only three electrode diameters were investigated, and also because the electrode size affected the fluidization as well as the electrical properties of the bed, it is impossible to determine quantitatively the relationship between the contact resistance and the electrode diameter. It only can be concluded that the contact resistance was not simply inversely proportional to the electrode surface area.

Effect of current

The results from the last four runs, as shown in Figure 30 indicate the contact resistance decreased with increasing current flow. This trend is more apparent than the effect of current on bed resistivity. A similar observation was also reported by Reed and Goldberger (42). Yuan's (51)

study of arcing in an electrofluid bed showed that more arcing was present in the vicinity of the center electrode than in the rest of the bed because the current density near the center electrode was larger. Since arcing is more likely to occur at higher current densities, the decrease of the contact resistance with increased currents may be due to the additional route for current flow provided by the arcing.

CONCLUSIONS AND RECOMMENDATIONS

Conclusions

1. As indicated from the computer simulation of the electric field in an electrofluid bed, the potential field in the vicinity of an electrode in the bed is distorted when there is contact resistance at the electrode surface.

2. Bed resistivity does not change significantly as the gas flowrate is increased until the minimum fluidization velocity is reached. As the gas flowrate is increased further, the bed resistivity increases rapidly to a peak value at the velocity where the bed is fully supported, and then decreases.

3. For a bed with a narrow distribution of particle sizes, bubbles form at the gas velocity where the bed is fully supported; this velocity is 1.2 times the minimum fluidization velocity. With a wide particle size distribution in the bed, the velocity at which the bed is fully supported is twice the minimum fluidization velocity and the bubbles form at a velocity between these two. In this case, the bed resistivity versus gas velocity curve exhibits a break point when bubbles form.

4. Bed resistivities of graphite beds are much smaller than those of calcined coke beds.

5. A calcined coke bed with a wide particle size distribution gives a bed resistivity much less than one with a narrow particle size distribution.

6. Bed resistivity decreases as current flow increases.

7. The semi-empirical correlation proposed for the bed resistivity in the fixed bed region seems successful; the variable, f_d, involved in the correlation is dependent only on the relative fluidization velocity and the type of bed material. f_d diminishes from one to zero as the gas flowrate goes from zero to the velocity where bubbles form in the bed, and in this gas flow range graphite beds consistently show a higher value of f_d than calcined coke beds. This difference is attributed to the fact that arcs form more easily in graphite beds.

8. Contact resistance generally increases as gas flowrate is increased, but shows an erratic behavior in the gas flow region between the minimum fluidization velocity and the velocity where the bed is fully supported for beds with a narrow particle size distribution.

9. The contact resistance at the electrode is strongly dependent on the electrode material; silicon carbide gives the largest contact resistance, followed by stainless steel, brass and graphite.

10. The contact resistance at the interface between the electrode and a graphite bed is less than that when a calcined coke bed is used. In the fixed bed region the ratio between the contact resistance and bed resistivity is the same for both beds, in other words, the contact resistance is proportional to the bed resistivity.

11. Contact resistance decreases as current density is increased.

12. Contact resistance decreases as the surface area of the electrode is decreased.

13. Two different effects of gas flowrate on contact resistance are observed. In the first case, the contact resistance rise sharply when the gas flowrate exceeds a value necessary to support the bed

and this pattern is shown by beds with a 0.5-inch diameter center electrode. With a 1.0-inch diameter center electrode, a large rise in contact resistance is not observed.

Recommendations

1. The bed resistivity should be measured at more current densities to find the limiting bed resistivity as an extrapolated value at zero current density. This limiting bed resistivity is considered to be the one when arcing is totally eliminated in the electrofluid bed and the conducting chains are the only mechanism for current flow. The semi-empirical correlation of this limiting bed resistivity would then show f_d dependent only on the relative fluidization velocity without any observed effect of bed material.

2. The semi-empirical correlation for bed resistivity could be extended beyond the gas flowrate where bubbles form when more information about the gas bubble phenomena are available.

3. Since bed resistivity is correlated with respect to the static bed resistivity in this investigation, more effort should be directed toward relating the static bed resistivity to the corresponding basic bed properties, like voidage and shape and size of bed particles in order to complete the correlation.

4. The contact resistance should be measured with other electrode materials to determine quantitatively the relationship between the contact resistance and the physical properties of the material. One

of the most possible properties is the softness of the electrode as indicated from the result of this investigation.

5. In order to develop a model which counts the causes of contact resistance, a two dimensional fluidization column seems necessary to be built for a visual observation of the fluidization condition around the electrode.

NOMENCLATURE

A	Cross-sectional area for current flow
a	Radius of center electrode
b	Radius of wall electrode
f	Volume fraction of dispersed phase
f_d	Volume fraction of the bed remained with the basic structure of settled bed
I	Current
K_c	Electrical conductivity of continuous phase
K_{cs}	Electrical conductivity of settled bed
K_d	Electrical conductivity of dispersed phase
K_m	Electrical conductivity of composite material
L	Bed height
L_s	Bed height of settled bed
n	Total number of particles present in the bed
ΔP	Pressure drop of fluidized bed
$(\Delta P)_{eq}$	Pressure drop which counterbalances the bed weight
R_b	Bed resistance
R_{ce}	Contact resistance at center electrode
R_{cw}	Contact resistance at wall electrode
r	Radial coordinate
U	Fluidization velocity
U_{br}	Fluidization velocity at which bubbles start to rise
U_{mf}	Minimum fluidization velocity
U_{rel}	Relative fluidization velocity, U/U_{mf}

V	Voltage drop between probe and wall electrode
V_a	Extrapolated voltage drop reading at r = a
V_b	Extrapolated voltage drop reading at r = b
V_o	Total voltage drop
V_p	Volume of particle
z	Axial coordinate
ϵ	Porosity of fluidized bed
ϵ_s	Porosity of settled bed
ρ_b	Bed resistivity
ρ_c	Contact resistivity
ϕ	Potential function
Ψ	Stream function

LITERATURE CITED

1. Ballain, M. D., and A. H. Pulsifer. 1970. Electrode temperature and resistance of an electrothermal fluidized bed. Chem. Eng. Symp., Ser. 66, 105:229-235.

2. Bruggeman, D. A. G. 1935. Berechnung verschiedener physikalischer Konstanten von heterogenen Substanzen. Ann. Physik. 24:636-664.

3. Buyevich, Y. A. 1974. On the thermal conductivity of granular materials. Chem. Eng. Sci. 29:37-48.

4. Chan, C. K., and C. L. Tien. 1973. Conductance of packed spheres in vacuum. ASME. Paper No. 73-HT-1.

5. Davidson, J. F., and D. Harrison. 1971. Fluidization. Academic Press, London.

6. De Graff, W. N. 1968. Cyanides from hydrocarbon. South African Chem. Proc., Ser. 3, 5:CP113-CP119.

7. Dirksen, H. A., and B. S. Lee. 1966. Balanced-pressure pilot reactors. Chem. Eng. Progr., Ser. 62, 6:98-99.

8. Fricke, H. 1924. A mathematical treatment of the electric conductivity and capacity of disperse systems. Phys. Rev. 24:575-595.

9. Glidden, H. J., and A. H. Pulsifer. 1968. Electrode contact resistance in a fluidized bed. Can. J. Chem. Eng., Ser. 46, 6:476-478.

10. Goldberger, W. M., J. E. Hanway, Jr., and B. G. Langston. 1965. The electrothermal fluidized beds. Chem. Eng. Progr., Ser. 61, 2:63-67.

11. Goldschmidt, D., and P. LeGoff. 1963. Resistance electrique des lit fluidises. I. Resistance moyennes de grains par air: Resultants preliminaries. Chem. Eng. Sci. 18:805-806.

12. Goldschmidt, D., and P. LeGoff. 1967. Electrical methods for the study of a fluidized bed of conducting particles. Trans. Inst. Chem. Eng. 45:T196-T204.

13. Graham, W., and E. A. Harvey. 1965. The electrical resistance of fluidized beds of coke and graphite. Can. J. Chem. Eng., Ser. 43, 3:146-149.

14. Graham, W., and E. A. Harvey. 1966. The electrical conductivity of fluidized beds of coke and graphite up to 1200°C. Can. J. Chem. Eng., Ser. 44, 1:17-20.

15. Hayakawa, T., W. Graham, and G. L. Osberg. 1964. A resistance probe method for determining local solid particle mixing rates in a batch fluidized bed. Can. J. Chem. Eng., Ser. 42, 3:99-103.

16. Holm, R. 1967. Electric contacts, 4th ed. Springer-Verlag, Berlin.

17. Johnson, H. S. 1961. Reactions in a fluidized coke bed with self-resistive heating. Can. J. Chem. Eng., Ser. 39, 3:145-147.

18. Johnson, H. S., and A. H. Anderson. 1961. Process for the preparation of carbon disulfide and for the desulfurization of coke: Assigned to Shawinigan Chemicals Limited, Montreal, Canada. U.S. Patent 3,009,781. November 21, 1961.

19. Johnson, H. S., and A. H. Anderson. 1960. Process for the preparation of carbon monoxide: Assigned to Shawinigan Chemicals Limited, Montreal, Canada. U.S. Patent 2,921,840. January 19, 1960.

20. Johnson, H. S., and A. H. Anderson. 1960. Process for the preparation of hydrocyanic acid: Assigned to Shawinigan Chemicals Limited, Canada. U.S. Patent 2,958,584. November 1, 1960.

21. Johnson, H. S., and A. H. Anderson. 1960. Process for the preparation of titanium tetrachloride: Assigned to Shawinigan Chemicals Limited, Montreal, Canada. U.S. Patent 2,948,587. August 9, 1960.

22. Johnson, H. S., and J. Reid. 1962. Process for the preparation of carbon disulfide: Assigned to Shawinigan Chemicals Limited, Montreal, Canada. U.S. Patent 3,034,863. May 15, 1962.

23. Jones, A. L., and T. D. Wheelock. 1968. The electrical resistivity of fluidized carbon particles: Determination of resistivity by the four-terminal method. Inst. Chem. Eng. Symp. Ser. 30:174-181.

24. Jones, A. L., and T. D. Wheelock. 1970. The electrical resistivity of fluidized carbon particles: Significant parameters. Chem. Eng. Symp. Ser., Ser. 66, 105:157-166.

25. Kennedy, K. J. 1962. Preparation of hydrocyanic acid: Assigned to Shawinigan Chemicals Limited, Quebec, Canada. U.S. Patent 3,032,396. May 1, 1962.

26. Kennedy, K. J., and N. R. Shine. 1963. Preparation of hydrogen cyanide: Assigned to Shawinigan Chemicals Limited, Quebec, Canada. U.S. Patent 3,097,921. July 16, 1963.

27. Knowlton, T. M. 1971. Components of interelectrode resistance in an electrofluid bed reactor. Ph.D. Thesis. Iowa State University.

28. Kossman, T. M. 1961. Process for heating beds of solid particles apouted with gas: Assigned to Shawinigan Chemicals Limited, Montreal, Canada. U.S. Patent 2,968,683. January 17, 1961.

29. Kunii, D., and O. Levenspiel. 1969. Fluidization Engineering. John Wiley and Sons, Inc., New York, New York.

30. Lee, B. S. 1970. Synthetic pipeline gas from coal by the HYGAS process. Paper presented at the American Power Conference, Chicago, April 21, 1970.

31. Lee, B. S., E. J. Pyrcioch, and F. C. Schora, Jr. 1968. The electrical resistivity of a high pressure fluidized bed. Paper presented at the 61st National Meeting of AIChE, Los Angeles, December 1, 1968.

32. Leva, M. 1959. Fluidization. McGraw-Hill, New York, New York.

33. Lord Rayleigh. 1892. On the influence of obstacles arranged in rectangular order upon the properties of a medium. Phil. Mag. 34:481-502.

34. Maxwell, J. C. 1881. A treatise on electricity and magnetism. 2nd ed. Vol. 1. Clarendon Press, Oxford.

35. Meredith, R. W., and C. W. Tobias. 1962. Chapter II: Conduction in heterogeneous system, Vol. 2, pages 15-47 in Meredith, R. W., and C. W. Tobias. Advances in electrochemistry and electrochemical engineering. Interscience Publishers, New York.

36. Miles, C. D., and F. M. Stephens, Jr. 1964. Fluidized bed method of producing phosphorus: Assigned to FMC Corp., Princeton, New Jersey. U.S. Patent 3,118,734. January 21, 1964.

37. Morse, P. M., and H. Feshbach. 1935. Methods of theoretical physics. Part II. McGraw-Hill, New York.

38. Noncatalytic reaction boosts HCN yields. 1961. Chem. Eng., Ser. 68, 19:72.

39. Orr, Clyde, Jr., and J. M. Dallavalle. 1954. Heat transfer properties of liquid-solid suspension. Chem. Eng. Symp., Ser. 50, 9:29-45.

40. Paquet, J. L., and P. B. Foulkes. 1965. Calcination of fluid coke in an electrically heated fluidized bed. Can. J. Chem. Eng., Ser. 43, 2:94-96.

41. Pulsifer, A. H., and T. D. Wheelock. 1972. Production of hydrogen from coal char in an electrofluid reactor. I & RC Process Design & Development 11:229-237.

42. Reed, A. K., and W. M. Goldberger. 1966. Electrical behavior in fluidized beds of conducting solids. Chem. Eng. Progr. Symp. Ser., Ser. 62, 67:71-75.

43. Sevryukov, V. N., and I. G. Martyushin. 1968. The total electrical resistance of a fluidized bed of electrically conducting granular material. International Chem. Eng., Ser. 8, 2:209-211.

44. Shine, N. B. 1971. Fluohmic process for hydrogen cyanide. Chem. Eng. Progr., Ser. 67, 2:52-57.

45. Smith, D. G. 1972. Electrical resistivity of high temperature fluidized carbon beds. M.S. Thesis. Iowa State University.

46. Spink, D. R., J. W. Cookston, and J. E. Hanway, Jr. 1964. The fluidized bed chlorination of zirconium-bearing materials. Paper presented at the Annual Meeting of American Inst. of Mining, Metall. and Petrol. Engrs., New York, February 1964.

47. Turner, J. C. R. 1972. The electrical conductivity of a liquid-fluidized bed. Presented at the Session on Fluidization Fundamentals, 72nd National Meeting of AIChE, St. Louis, Missouri, May 21, 1972.

48. Wickenden, L., and S. A. W. Okell. 1927. Process and apparatus for making decolorizing carbon. U.S. Patent 1,634,478. July 5, 1927.

49. Winkler, F. 1932. Production of water gas: Assigned to I. G. Farbenindustrie. U.S. Patent 1,857,799. May 10, 1932.

50. Yovanovich, M. M. 1973. Apparent conductivity of glass microspheres from atmospheric pressure to vacuum. Presented at the ASME-AIChE Heat Transfer Conference, Atlanta, Ga., August 5, 1973.

51. Yuan, E. K. C. 1973. The electrical properties of a fluidized bed. Ph.D. Thesis. Iowa State University.

52. Zenz, F. A., and D. F. Othmer. 1960. Fluidization and fluid particle system. Reinhold Publishing Corp., New York, New York.

53. Zheltov, A. I., S. S. Zabrodsky, and V. A. Borodulya. 1972. Electrical properties of fluidized and settled beds of graphite particles at temperature up to 2500°C. Presented at the Session on Fluidization Fundamentals, 72nd National Meeting of AIChE, St. Louis, Missouri, May 21, 1972.

ACKNOWLEDGMENTS

The author would like to express his appreciation to Dr. A. H. Pulsifer and Dr. T. D. Wheelock who suggested this project and provided valuable guidance throughout the investigation. Appreciation is also expressed to Dr. L. E. Burkhart for his assistance in using the PDP-8 computer to collect experimental data.

The Office of Coal Research is also gratefully acknowledged for its financial support of this investigation.